iScience

CellPress
OPEN ACCESS

Review

Controllable growth of two-dimensional materials on noble metal substrates

Yang Gao,[1] Yang Liu,[2,3,*] and Zheng Liu[1,4,5,*]

SUMMARY

Chemical vapor deposition (CVD) is a promising approach for the controllable synthesis of two-dimensional (2D) materials. Many studies have demonstrated that the morphology and structure of 2D materials are highly dependent on growth substrates. Hence, the choice of growth substrates is essential to achieve the precise control of CVD growth. Noble metal substrates have attracted enormous interest owing to the high catalytic activity and rich surface morphology for 2D material growth. In this review, we introduce recent progress in noble metals as substrates for the controllable growth of 2D materials. The underlying growth mechanism and substrate designs of noble metals based on their unique features are thoroughly discussed. In the end, we outline the advantages and challenges of using noble metal substrates and prospect the possible approaches to extend the uses of noble metal substrates for 2D material growth and enhance the structural controllability of the grown materials.

INTRODUCTION

Large-area, high-quality, and uniform two-dimensional (2D) materials are highly desired for their future applications in diverse fields (Choi et al., 2017; Fiori et al., 2014; Manzeli et al., 2017; Novoselov et al., 2012). Several approaches have been developed for preparing 2D materials, such as micromechanical cleavage (Novoselov et al., 2005), liquid exfoliation (Coleman et al., 2011), wet-chemical synthesis (Tan and Zhang, 2015), and molecular beam epitaxy (Park et al., 2010). Compared with the methods mentioned above, chemical vapor deposition (CVD) shows excellent structural controllability of grown 2D materials with satisfactory quality and great potential for future large-area applications (Chen et al., 2018; Zhao et al., 2019). As a typical bottom-up method, CVD allows sufficient design space and precise control over its synthesis factors, which are difficult to achieve by a top-down method. Notably, growth substrate directly determines the growth mechanism of a specific growth process, which differs considerably from many other growth factors, such as growth temperature, growth time, and gas flow rate. Therefore, the rational selection and design of the growth substrate are essential for the highly controllable growth of 2D materials.

Various metals and nonmetals have been explored as growth substrates for the large-area preparation of 2D materials (Qin et al., 2020). The representative substrates used for growing graphene and 2D hexagonal boron nitride (*h*-BN) layers are Cu (Kim et al., 2012; Li et al., 2009) and Ni (Shi et al., 2010; Yu et al., 2008), while inert nonmetal substrates (Wang et al., 2020) such as SiO_2 (Lee et al., 2012b, 2013) and sapphire (Lee et al., 2013) are widely used for 2D transition metal dichalcogenide (TMDC) growth. However, poor quality, low growth rate, and non-uniform structure of the obtained materials are still insurmountable problems in using these substrates. In contrast, the excellent catalytic ability and fast diffusion of precursor atoms on the noble metal substrates, i.e., Pt (Gao et al., 2012; Ma et al., 2019) and Au (Chen et al., 2019; Gao et al., 2015, 2017), allow very few defects, ultrafast growth and uniform structure in the grown 2D layers. For instance, graphene grown on Pt can achieve ~3 mm large single-crystal domains without sacrificing carrier mobility (Ma et al., 2014b). Inch- and wafer-scale *h*-BN films can be synthesized on Pt (Gao et al., 2013; Kim et al., 2013; Park et al., 2014) and Au (Lee et al., 2018) substrates, respectively. MoS_2 (Shi et al., 2014; Yang et al., 2020), $MoSe_2$ (Wu et al., 2021), WS_2 (Gao et al., 2015), and WSe_2 (Gao et al., 2017) on Au show high uniformity in thickness over entire substrate areas.

This review categorizes the noble metal substrates used for CVD growth of 2D materials into three critical aspects by designs, i.e., homogeneous, heterogeneous, and surface-engineered substrates (Figure 1). First, we would like to introduce two main structures of noble metal substrates, i.e., the homogeneous

[1]School of Materials Science and Engineering, Nanyang Technological University, Singapore 639798, Singapore

[2]Cyber Security Research Centre, Nanyang Technological University, Singapore 639798, Singapore

[3]School of Computer Science and Engineering, Nanyang Technological University, Singapore 639798, Singapore

[4]CINTRA CNRS/NTU/THALES, UMI 3288, Research Techno Plaza, Singapore 637553, Singapore

[5]School of Electrical and Electronic Engineering, Nanyang Technological University, Singapore 639798, Singapore

*Correspondence: yangliu@ntu.edu.sg (Y.L.), z.liu@ntu.edu.sg (Z.L.)

https://doi.org/10.1016/j.isci.2021.103432

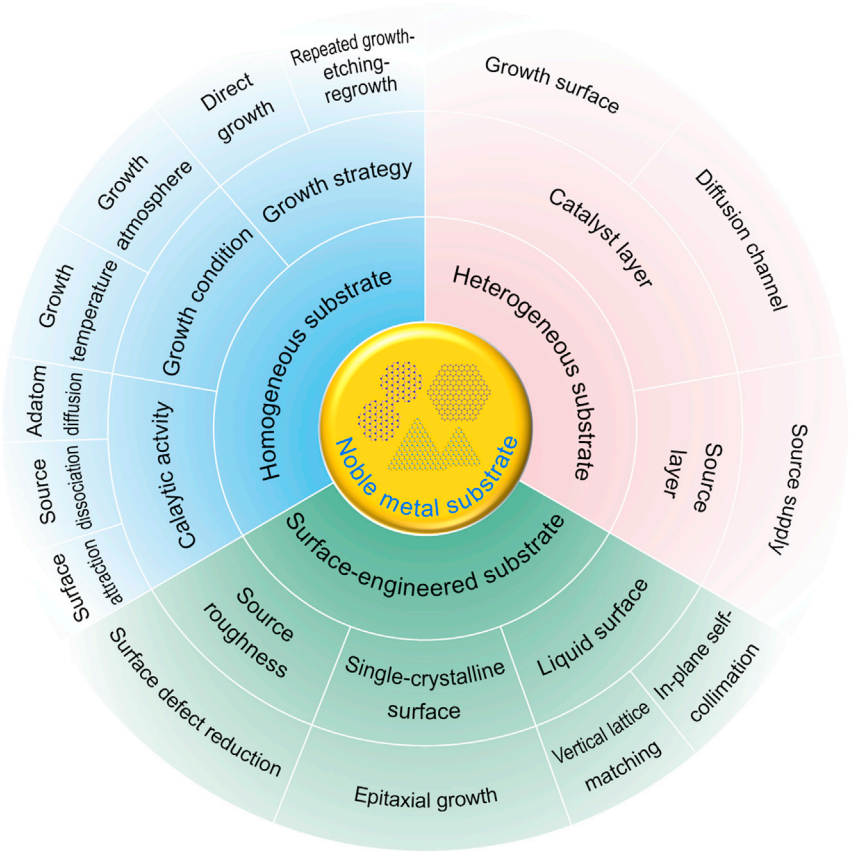

Figure 1. Overview of designed substrates based on noble metals for the controllable CVD growth of 2D materials

noble metal substrate containing only a noble metal and the heterogeneous substrate containing both a catalyst-metal layer and a source-metal layer. The fundamental growth mechanisms underlying diverse substrate designs are also discussed. Next, surface engineering is investigated to enhance the structural controllability of 2D materials. Finally, the properties and potential applications of the grown 2D materials using noble metal substrates are summarized. In addition, the challenges remaining in CVD growth using noble metal substrates are particularly pointed out, and the prospective routes are proposed correspondingly.

The epitaxial growth of atomically thin layers was achieved on diverse metal substrates in ultrahigh vacuum (UHV) systems (Corso et al., 2004; Gamo et al., 1997; Helveg et al., 2000; Nagashima et al., 1995) many years ago, even before isolating graphene from graphite in 2004 (Novoselov et al., 2004). Such growth requires complicated growth equipment and follows growth mechanisms different from those of ambient-pressure and low-pressure CVD methods. Therefore, this review only focuses on CVD growth under ambient or low pressure and does not extend to vapor-phase growth in UHV systems for concision.

HOMOGENEOUS NOBLE METAL SUBSTRATE

This section discusses the design strategies of using only a noble metal as the substrate for CVD growth of various 2D materials, including graphene, *h*-BN, and TMDCs. The unique features of noble metals allow growth mechanisms different from those in CVD growth on nonmetal and other metal substrate materials. Besides selecting growth substrates, the matching growth conditions and strategies are also essential to take the best advantage of noble metals for the high structural controllability of 2D products.

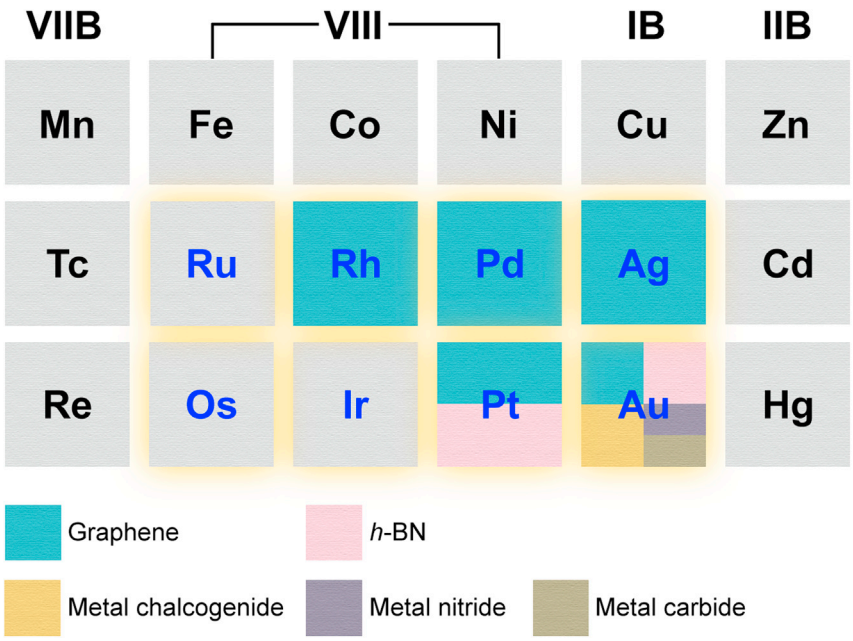

Figure 2. Periodic table of the known 2D materials that can grow on noble metal substrates by CVD methods
All noble metal elementals are indicated in blue. Graphene, *h*-BN, metal chalcogenides, metal nitrides, and metal carbides are marked with different colors. Note that this table excludes the 2D materials grown in UHV.

Noble metal for graphene growth

Noble metals refer to eight chemical elements shown in Figure 2, including Au, Ag, and six platinum-group elements (Pt, Ir, Rh, etc.). As the name implies, they are well known for their "noble" characters distinct from non-noble metals, not only high price but also, more importantly, excellent corrosion resistance at ambient conditions and in more complex environments, such as CVD growth atmospheres and oxidizing acids. The latter, i.e., excellent corrosion resistance, does not necessarily mean that noble metals are not involved in multiple chemical reactions but instead is attributed to the difficulty in forming stable compounds between noble metals and nonmetal elements. As a result, noble metals can be avoided from poisoning by nonmetal elements in catalytic processes and thus serve as high-performance catalysts. During the whole growth process of the CVD growth, the noble metals can maintain efficient and sustainable catalytic activity without degradation because no stable compounds form on their surfaces at high temperatures. For instance, phase diagrams and many studies show that no carbide exists in the Pt-C and Au-C systems; noble metal nitrides can only be synthesized under extreme conditions (e.g., 45–50 GPa and exceeding 2,000 K) (Gregoryanz et al., 2004; Horvath-Bordon et al., 2006), or remain undetected; the decompositions of Pt_2B and AuB_2 occur over 950°C and over 1000°C, respectively. Therefore, it is possible to use Pt and Au as the substrates for the CVD growth of graphene and 2D *h*-BN at reasonable temperatures. Also, the absence of sulfide, selenide, and telluride in Au-S, Au-Se, and Au-Te systems above certain temperatures (e.g., 500°C), respectively, indicates that Au can be a candidate as the substrate for 2D TMDC growth.

The first effort to use noble metal substrates for CVD growth of 2D materials was made in the graphene growth on Pt (Figures 3A and 3B) (Gao et al., 2011, 2012; Kang et al., 2009; Yong and Hahn, 2011). Correspondingly, we commence the review and discussion on the catalytic behavior of noble metals in the CVD growth of graphene and then extend to that of 2D materials beyond graphene. Before then, Cu (Li et al., 2009) and Ni (Kim et al., 2009; Yu et al., 2008) had been used for growing monolayer and few-layer graphene, respectively, which had successfully achieved the controllable synthesis of graphene with both scalability and uniform thickness to some degree. However, the crystalline quality was still incomparable with that of mechanically exfoliated graphene. Point defects (Banhart et al., 2011), grain boundaries (Yu et al., 2011), wrinkles (Chae et al., 2009), and other defects are detrimental to the electrical performance of graphene-based devices. Thus, the carrier mobility of the CVD-grown graphene (Kim et al., 2009; Li et al., 2009; Reina et al., 2009) is still an order of magnitude lower than those of the samples prepared by mechanical exfoliation (Chen et al., 2008; Morozov et al., 2008). Therefore, it was desirable to explore new growth

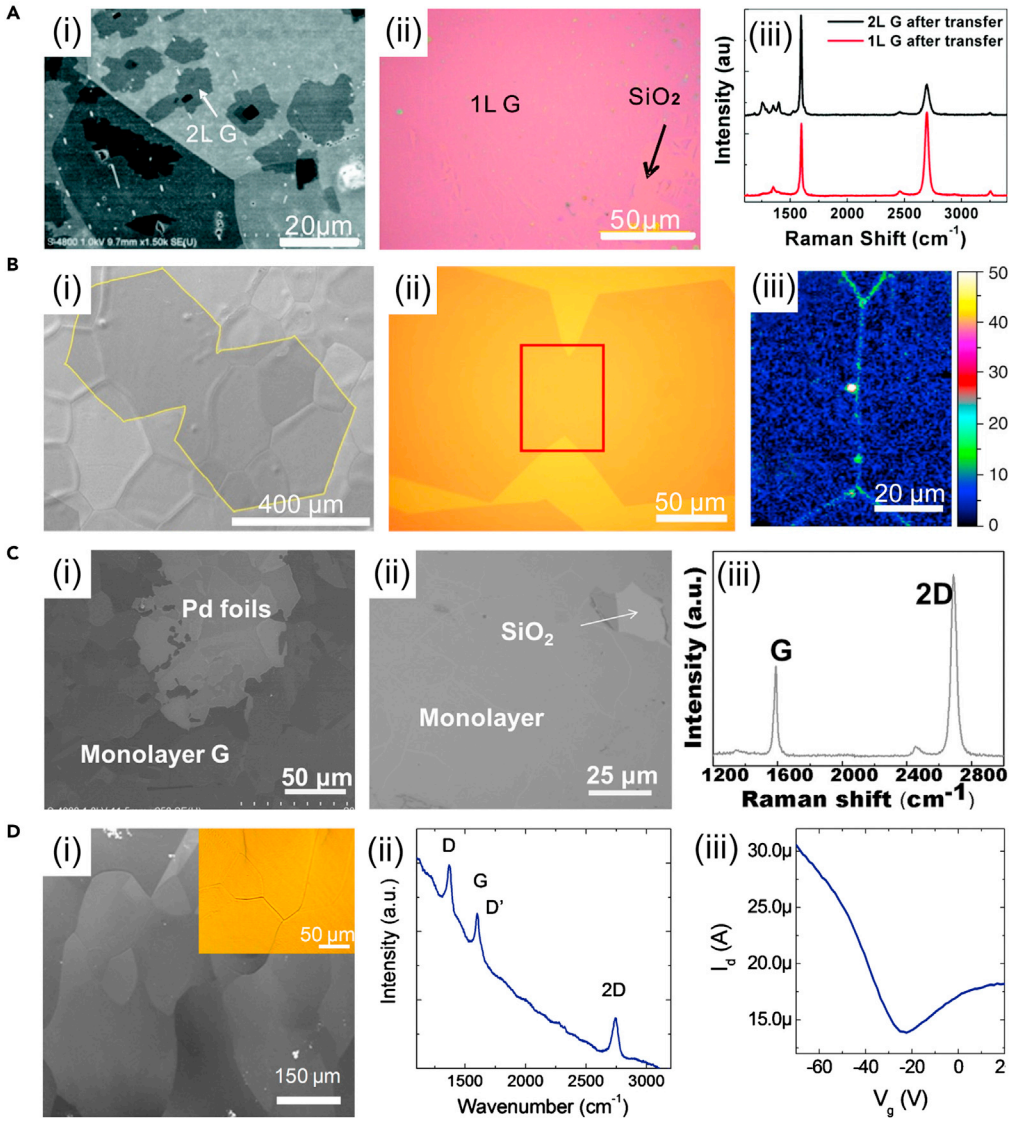

Figure 3. Comparison of the graphene growth on different polycrystalline noble metals

(A) Monolayer graphene with adlayers grown on Pt in a hydrogen-moderate environment. (i) SEM image of monolayer and bilayer graphene on a Pt foil. (ii) Optical microscopy (OM) image of monolayer graphene transferred on SiO_2/Si. (iii) Raman spectra of monolayer and bilayer graphene after transfer on SiO_2/Si. Reprinted with permission from Gao et al. (2011). Copyright 2011, American Chemical Society.

(B) Milliliter-sized monolayer graphene grains grown on Pt in a hydrogen-rich environment. (i) SEM image of monolayer graphene grains on a Pt foil. (ii) OM image of two coalesced graphene grains transferred on SiO_2/Si. (iii) Raman mapping of the *D* peak intensity of the joined area of two grains indicated by a red box in (ii). Reprinted with permission from Gao et al. (2012). Copy right 2012, Springer Nature.

(C) Monolayer graphene grown on Pd. (i) SEM image of monolayer graphene on a Pt foil. (ii) OM image of monolayer graphene transferred on SiO_2/Si. (iii) Representative Raman Spectrum of the graphene sample in (ii).Reprinted with permission from Ma et al. (2014a). Copyright 2014, John Wiley & Sons, Inc.

(D) Monolayer graphene grown on Au. (i) SEM and OM (inset) images of monolayer graphene on an Au foil. (ii) Raman spectra of the graphene transferred on SiO_2/Si. (iii) Transfer characteristic of a graphene-based FET. Reprinted with permission from Oznuluer et al. (2011). Copyright 2011, American Physical Society.

substrates beyond Cu and Ni. Many other non-noble metal substrates, such as Fe and Co (Liu et al., 2011), have shown unspectacular layer-number controllability of graphene, even worse than Cu and Ni. Several noble metals (Gao et al., 2011, 2012; Liu et al., 2012b; Ma et al., 2014a, 2014b) have been selected as

candidates for better control of graphene growth, highlighted with Pt substrates (Gao et al., 2012; Ma et al., 2014b). Gao et al. (Gao et al., 2012) demonstrated the growth of large-area single-crystalline graphene by using Pt foils, for the first time increasing graphene domain sizes to a millimeter scale, as shown in Figure 3B. The faster growth rate and broader growth windows in the graphene growth on Pt than on Cu indicate that Pt has higher catalytic activity than Cu for dissolving methane (Au et al., 1999) and H_2 (Gomez et al., 2011). More importantly, the extracted mobility of the device based on Pt-grown graphene (Gao et al., 2012) shows superior mobility (Gao et al., 2012) compared to Cu- (Li et al., 2009) and Ni- (Kim et al., 2009) grown graphene measured under similar conditions. Besides Pt, Rh (Liu et al., 2012b) and Pd (Figure 3C) (Ma et al., 2014a) have also been demonstrated to grow high-quality continuous graphene films by segregation growth rather than surface-mediated growth using Pt (Gao et al., 2011, 2012). Monolayer graphene can also be obtained on Au, but the crystalline quality is very poor, indicated by a strong *D* peak and low mobility ~20 $cm^2 V^{-1} s^{-1}$ (Figure 3D) (Oznuluer et al., 2011).

Overall, the above explorations of noble metal substrates have demonstrated that not all but several noble metal substrates have outstanding catalytic activity for graphene growth. It is worth noting that graphene formation involves both hydrocarbon dissociation and graphitization on the substrate surface. The former can occur on the surfaces of multiple transition metals. However, the catalytic activity of different noble metals varies considerably in this step. Theoretical studies show that Pt is more active than Cu and Ni (Au et al., 1999; German and Sheintuch, 2013; Nave and Jackson, 2009) in methane dissociation, and such catalytic dissociation is almost negligible on Ag and Au because of high activation energy (Au et al., 1999; German and Sheintuch, 2013). Nevertheless, this cannot fully explain why Au can grow monolayer graphene but only with poor quality. The growth temperature for graphene is typically 800–1100°C, and methane spontaneously decomposes at such a high temperature. However, the dissociation productions, i.e., active carbon species such as carbon dimmers or chains, cannot stay long enough on the Au surface to stabilize the sp^2 carbons clusters (Raty et al., 2005). Thus, the obtained graphene contains amorphous regions shown as a strong *D* peak (Oznuluer et al., 2011).

Therefore, the substrate design is not just selecting noble metals with good catalytic activity. Deeper understandings of growth mechanisms are required to take advantage of these highly active noble catalysts and thus to achieve better control of the quality and structure of the obtained graphene. For example, in contrast to Au, Pt has both vigorous catalytic activity in methane dissociation (German and Sheintuch, 2013; Nave and Jackson, 2009) and the formation of sp^2-bonded carbon atoms (Hamilton and Blakely, 1980). However, excess active carbon species generated by Pt may also lead to two problems. First, the unresponsive graphitization of these abundant carbon species generates non-sp^2 defects, shown as a notable *D* peak in the Raman spectrum (Ferrari et al., 2006; Gao et al., 2011; Sun et al., 2014). Second, the relatively high carbon solubility in Pt (still lower than that in Ni) can lead to the dissolution and segregation of carbon atoms after sufficient feeding of active carbon species.

Consequently, the layer control of graphene on Pt may be difficult compared with less active non-noble metals in methane dissociation (Sun et al., 2014), and thus the grown monolayer graphene may have adlayers (Gao et al., 2011), as shown in Figure 3A. To mitigate this problem, another essential catalytic activity of Pt, i.e., H_2 dissociation (Gomez et al., 2011), should also be considered. The catalytic activity of H_2 dissociation is much stronger on Pt than on Cu and many other noble metals. Therefore, active hydrogen atoms can passivate the overfeeding of carbon species in Pt and etch graphene adlayers, leading to the surface growth of monolayer graphene and a reduction of the nucleation density. Therefore, a sufficient H_2 supply is introduced in the growth process of graphene to achieve quasi-equilibrium conditions for better control of the thickness and size of graphene grains (Gao et al., 2012; Wang et al., 2018). More importantly, disordered carbon species can be etched away in a hydrogen-rich environment. Ma et al. developed a growth and repeated etching-regrowth (G-rE-RG) strategy to achieve both large-area single-crystal graphene grains and excellent electrical performance compared to mechanically exfoliated samples (Figure 4) (Ma et al., 2014b). In this case, hydrogen etching dramatically reduced the nucleation density by removing the domains with relatively more defects. Then domains with fewer defects continued to grow by increasing methane flows. By delicately balancing the flow rate ratio of methane to H_2, ~3 mm defect-free graphene single crystals were finally obtained (Figure 4E) and showed very high carrier mobility up to 13,000 $cm^2 V^{-1} s^{-1}$ measured under ambient conditions. Both the sizes and crystalline quality of the obtained graphene grains increased compared with those of the grains directly grown on Pt (Gao et al., 2012; Ma et al., 2014b) without a hydrogen-etching process. Therefore, optimizing growth parameters and adopting

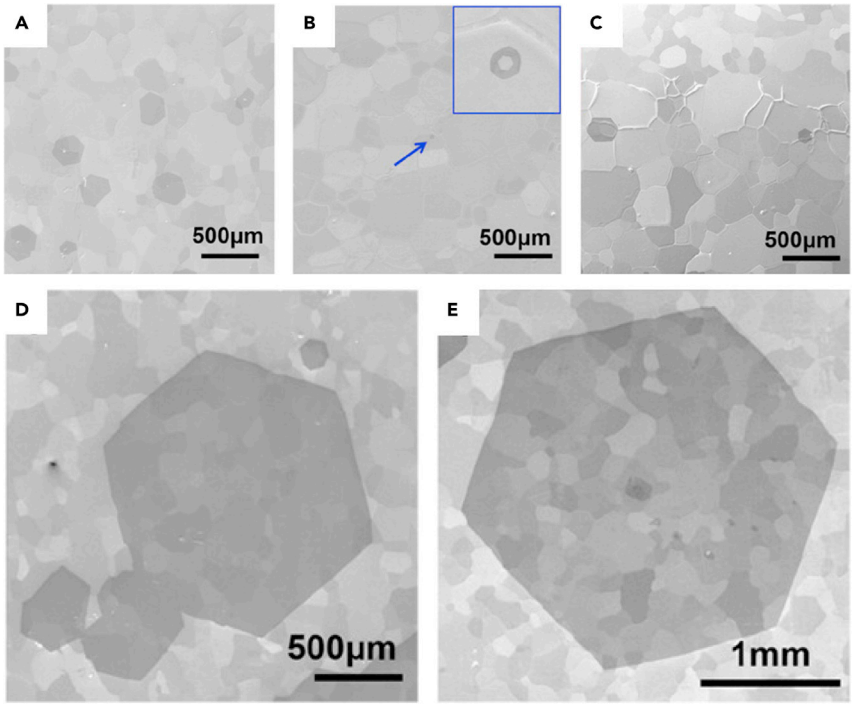

Figure 4. Morphology evolution of graphene domains at different stages during a G-rE-RG process on polycrystalline Pt

(A–C) Graphene domains at (A) the initial growth, (B) the sequential etching, and (C) the regrowth stages in the first etching-regrowth (E-RG) cycle.

(D and E) Millimeter-sized graphene domains after (D) the second and (E) the third E-RG cycles. Reprinted with permission from Ma et al. (2014b). Copyright 2014, American Chemical Society.

rational growth strategies are also essential for the precise control of graphene growth on noble metals and the following cases of other 2D materials.

Noble metal for 2D *h*-BN growth

As with the CVD growth of graphene, the metals initially used for graphene growth, i.e., Cu (Kim et al., 2012; Song et al., 2010) and Ni (Chatterjee et al., 2011; Shi et al., 2010), were soon explored for 2D *h*-BN growth since its sp^2-hybridized hexagonal honeycomb structure is very similar to that of graphene. However, it is still challenging to precisely control *h*-BN thickness over a large area (Chatterjee et al., 2011; Guo et al., 2012; Ismach et al., 2012; Shi et al., 2010; Song et al., 2010). For instance, Cu can be used to grow *h*-BN monolayers with micrometer-sized domains only under low pressure (Kim et al., 2012) or 2–5-layer *h*-BN films under atmospheric pressure (Song et al., 2010). On the other hand, 2D *h*-BN grown on Ni are multi-layers with non-uniform thickness using ambient-pressure CVD (APCVD) or low-pressure CVD (LPCVD) (Chatterjee et al., 2011; Ismach et al., 2012; Shi et al., 2010). Inspired by the impressive catalytic ability in graphene growth, both Pt (Gao et al., 2013; Kim et al., 2013; Park et al., 2014) and Au (Lee et al., 2018; Tan et al., 2020) were also chosen as substrates for 2D *h*-BN growth and show excellent controllability of thickness and defects. Importantly, continuous monolayer *h*-BN films over 1 inch can be grown on Pt foils by both APCVD and LPCVD methods (Gao et al., 2013; Kim et al., 2013; Park et al., 2014) shown in Figure 5, indicating a wider growth window for *h*-BN monolayers on Pt than on Cu and Ni.

Interestingly, an increase of precursor concentration in the rational range leads to the formation of uniform *h*-BN layers seamlessly stitched with bilayer domains on Pt (Figures 5B and 5D) (Gao et al., 2013), rather than losing thickness control of 2D *h*-BN with prolonging growth time (Ismach et al., 2012). Besides Pt, Au was also demonstrated for 2D *h*-BN growth (Lee et al., 2018; Tan et al., 2020). The migration barrier for B and N atoms on Au is much lower than that on many other metals (i.e., Cu, Ni, Pt, Pd), allowing Au to act as an excellent catalyst for 2D *h*-BN growth (Hu et al., 2015). Similar to the 2D *h*-BN grown on Pt,

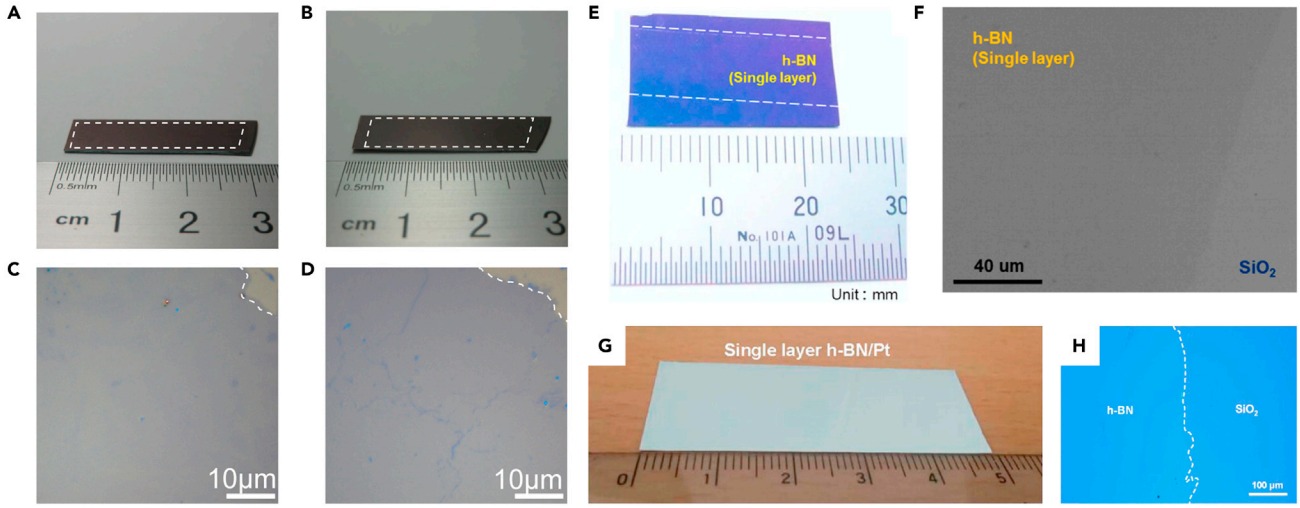

Figure 5. 2D *h*-BN growth on polycrystalline Pt using ammonia borane and borazine

(A–D) APCVD-grown monolayer and bilayer *h*-BN films using Pt and ammonia borane. (A and B) photography and (C and D) OM images of (A and C) monolayer and (B and D) bilayer *h*-BN films transferred on SiO_2/Si. Reprinted with permission from (Gao et al., 2013). Copyright 2013, American Chemical Society.

(E and F) LPCVD-grown monolayer *h*-BN films using Pt and ammonia borane. (E) Photography and (F) OM images of monolayer *h*-BN film transferred on SiO_2/Si. Reprinted with permission from Kim et al. (2013). Copyright 2013, American Chemical Society.

(G and H) APCVD-grown monolayer *h*-BN films using Pt and borazine. (G) Photography of monolayer *h*-BN on a Pt foil and (H) OM image of monolayer *h*-BN film transferred on SiO_2/Si. Reprinted with permission from Park et al. (2014). Copyright 2014, American Chemical Society.

h-BN films with tunable thickness from 3.5 to 10.6 nm can be selectively grown on Au by changing the feedstock mass (Tan et al., 2020). It is fascinating to note that the wafer-scale single-crystal *h*-BN monolayer films can be grown on liquid Au (Lee et al., 2018). This method is related to the significant roles of surface morphology in *h*-BN growth and will be thoroughly discussed in the Surface-engineered Substrate Section.

It is essential to point out that the careful use of precursors is also indispensable for achieving the high-quality and uniform growth of 2D *h*-BN after selecting the highly catalytic substrates. Unlike graphene, an elemental carbon, *h*-BN comprises two elements, i.e., B and N, and therefore it is challenging to achieve 1:1 stoichiometry of B and N atoms in the final 2D *h*-BN product. To this end, single-source precursors, such as ammonia borane (borazane) and borazine, are used in the CVD growth of 2D *h*-BN (Figure 5). The decomposition products of ammonia borane are borazine, monomeric aminoborane, and H_2 (Wolf et al., 2000), and actually, the effective source used for 2D *h*-BN growth is still borazine. Borazine turns to *h*-BN by gradually losing hydrogen atoms without breaking sp^2-hydridized B-N bonds at high temperatures (Fazen et al., 1995). Therefore, the grown 2D *h*-BN preserves a 1:1 atomic ratio of B to N. However, borazine, isostructural with benzene, is a chemically unstable, highly volatile liquid. Therefore, a cold trap is necessary for the safe use of borazine as a precursor for CVD growth (Park et al., 2014). Alternatively, ammonia borane, a well-known hydrogen storage material (Demirci, 2017), is very stable at room temperature and more promising for scale-up production of 2D *h*-BN films. However, a by-product from ammonia borane, i.e., monomeric aminoborane, polymerizes into poly-aminoborane, followed by incomplete dehydrogenation. Finally, many nanoparticles appear on 2D *h*-BN (Kim et al., 2012; Lee et al., 2012a). Besides directly using clean but unstable precursor borazine (Park et al., 2014), Gao et al. (Gao et al., 2013) demonstrated a simple strategy to use ammonia borane free of nanoparticles. A cellulose acetate filter (separated from a cigarette) placed after the precursor heater can effectively remove these nanoparticles and prevent the contamination of growth substrates by nanoparticles. Similar methods were also widely used for the clean growth of 2D *h*-BN from ammonia borane (Han et al., 2014; Wen et al., 2015).

Noble metal for 2D TMDC growth

Au is the only known noble metal widely used for 2D TMDC growth, now showing its multiple unique advantages in catalytic growth. The CVD growth of 2D TMDCs was first achieved on SiO_2/Si by Lee et al. (Lee et al., 2012b) in 2012. This pioneer report (Lee et al., 2012b) also mentioned the UHV epitaxial growth of

MoS_2 on Au (Helveg et al., 2000) but considered it an overcomplicated technique compared with that on SiO_2/Si. In the following two years, SiO_2/Si and other inert nonmetal substrates were widely investigated for the CVD growth of diverse 2D TMDCs (Gutiérrez et al., 2013; Huang et al., 2014; Lee et al., 2013; Najmaei et al., 2013; Wang et al., 2014; van der Zande et al., 2013). MoS_2 monolayers grown on Au were reported as early as 2000 (Helveg et al., 2000) and were identified as excellent catalysts for hydrogen evolution reaction (HER) by Jaramillo et al. in 2007 (Jaramillo et al., 2007). In 2014, Shi et al. first reported the LPCVD growth of MoS_2 on Au foils and also explored the HER applications of the MoS_2/Au hybrid catalyst (Shi et al., 2014). Their CVD-grown MoS_2 on Au is strictly monolayer domains with tunable sizes from ~200 nm to ~50 μm by changing growth temperatures, and the MoS_2 growth follows a surface growth mechanism (Figures 6A–6C). Indeed, HER applications do not require 2D materials with high crystalline quality, large area grains, or uniform thickness since they have fewer active sites for HER (Liu et al., 2017). Nevertheless, the results of the strictly monolayer MoS_2 flakes grown on Au are remarkably different from those of the MoS_2 flakes with adlayers grown on SiO_2/Si (Lee et al., 2012b, 2013), suggesting that Au may play a unique catalytic role in MoS_2 formation.

On the other hand, Au can also grow few-layer MoS_2 by combining surface alloying and sulfurization, as shown in Figures 6D–6F (Song et al., 2014). A Mo-Au surface alloy formed after sufficiently feeding Mo source under atmospheric pressure and then turned into MoS_2 on the top of Au by sulfidation (Song and Choi, 2019). Bilayer to trilayer MoS_2 continuous films (Figure 6F) or desired patterns can be feasibly obtained over a large area. However, the carrier mobility of field-effect transistors (FETs) based on the grown MoS_2 is as low as 0.004 $cm^2V^{-1}s^{-1}$, indicating an unsatisfactory crystal quality. Precisely speaking, this method is classified as thermally assisted conversion (TAC), but with an extra step, i.e., the diffusion of source-metal atoms before conversion, compared with conventional TAC from Mo (Kong et al., 2013; Zhan et al., 2012) or MoO_3 (Lin et al., 2012) films into MoS_2. The role of Au substrates, in this case, is to reserve a limited amount of Mo atoms for the formation of atomically thin MoS_2 films rather than bulks (Song and Choi, 2019). However, whether Au had the catalytic activity involved in the chemical reaction during the 2D TMDC growth remained elusive.

Gao et al. reported the self-limited growth of monolayer WS_2 on Au foils (Figures 6G and 6H) (Gao et al., 2015). Both experimental studies and theoretical calculations revealed the surface-catalytic mechanism in this method. Unlike the MoS_2 growth on Au, the extremely low solubility of W in Au substrates enables no excess W atoms to dissolve in and segregate on Au even under atmospheric pressure. This unique feature, together with the catalytic activity of Au, allows the surface growth of strictly monolayer WS_2 by using a low concentration of precursors. Thus, both WS_2 adlayers and excess nuclei are intensively suppressed during the growth process. As a result, millimeter-sized single-crystal domains (Figure 6G) and ~2-inch continuous films can form on Au foils under optimized conditions. Au substrates have also been used to grow large-area single-crystal WSe_2 domains (Figure 6I) and show the unique ability to speed up the growth rate of WSe_2 by several orders of magnitude faster than those of conventional growth of 2D TMDCs on SiO_2/Si and other nonmetal substrates (Gao et al., 2017). Although the WSe_2 grows on Au is up to ~26 μms^{-1} at 950°C, the extract carrier mobility ~143 $cm^2V^{-1}s^{-1}$ indicates that the quality is not sacrificed even after the growth at a remarkably high rate. Instead, the electrical performance of Au-grown WSe_2 is within the best values of both CVD-grown and mechanically exfoliated monolayer WSe_2 (Li et al., 2015; Liu et al., 2013; Wu et al., 2016).

Indeed, 2D TMDCs can directly grow on multiple inert nonmetal substrates by CVD, indicating that the chemical reaction can occur without catalyst assistance at growth temperatures. After the formation of monolayer TMDCs, the non-catalytic areas of the substrates, including both top surfaces of monolayer TMDCs and bared areas of nonmetal substrates, are exposed to the same species of precursors, which are directly from the growth atmosphere without catalytic dissociation. Thus, the nucleation and expansion of adlayer domains can also occur on top of the first layers, which are simultaneously growing. Therefore, it is challenging to retain the monolayer structure of 2D TMDCs on inert nonmetal substrates during CVD growth.

The catalytic ability of Au substrates provides a new route for the precise control of 2D TMDC growth. It is worth mentioning that it takes considerable energies of 3.37, 2.8, and 2.2 eV to dissociate S_2, Se_2, and Te_2 dimers into S, Se, and Te atoms, respectively (Somayajulu, 1960). Many other experimental studies have also confirmed the energy barriers of forming active single chalcogen atoms from vapors, although only

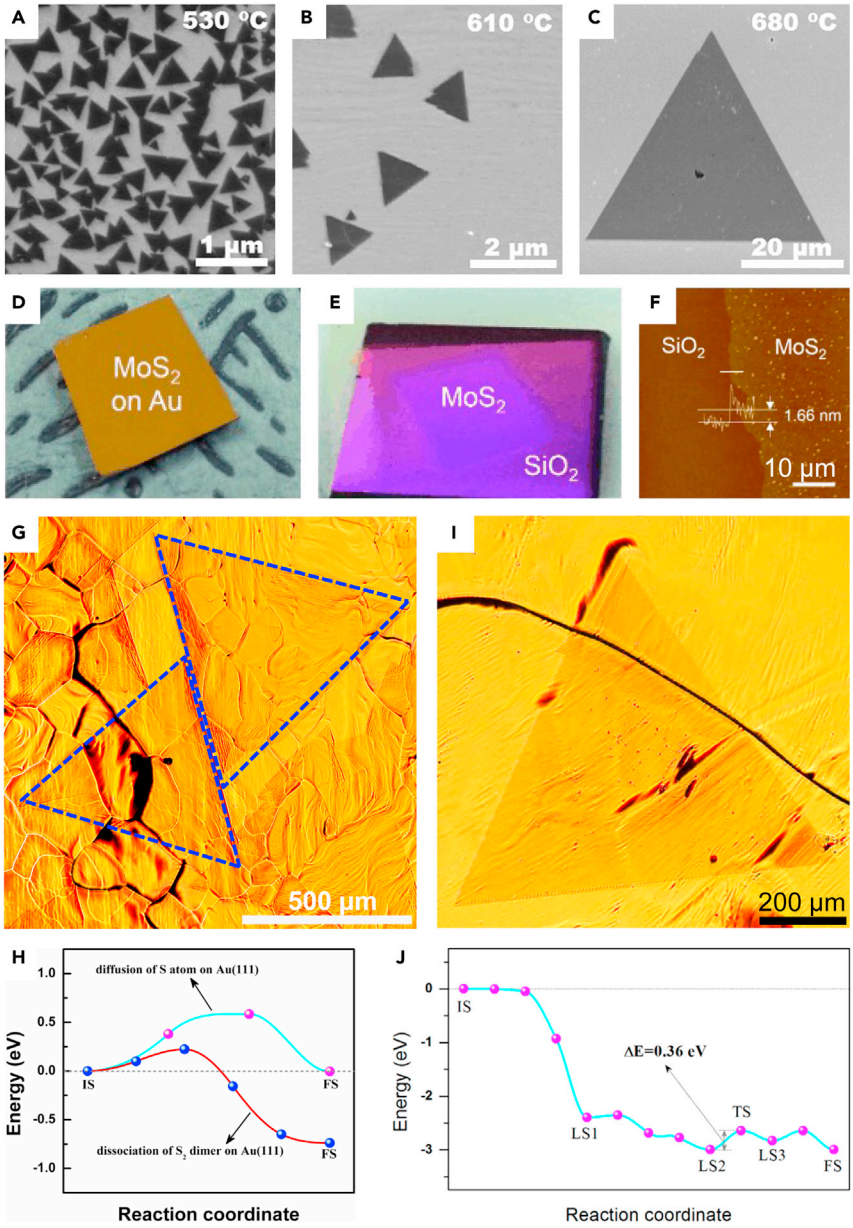

Figure 6. 2D TMDC growth on polycrystalline Au

(A–C) LPCVD-grown monolayer MoS_2 domains on Au foils with tunable sizes under distinct growth temperatures. Reprinted with permission from (Shi et al., 2014). Copyright 2014, American Chemical Society.

(D–F) APCVD-grown few-layer MoS_2 films on Au by the sulfurization of the Mo-Au surface alloy. Photography of (D) as-grown few-layer MoS_2 film on Au and (E) transferred sample on SiO_2/Si. (F) Atomic force microscopy (AFM) image showing the thickness of MoS_2 film. Reprinted with permission from Song et al. (2014). Copyright 2014, John Wiley & Sons, Inc.

(G) APCVD-grown millimeter-sized large-area monolayer WS_2 single crystals on Au.

(H) DFT calculated the minimum energy path for the dissociation of S_2 dimers into S atoms and the S atom diffusion on Au(111). Reprinted with permission from Gao et al. (2015). Copyright 2015, Springer Nature.

(I) APCVD-grown millimeter-sized large-area monolayer WSe_2 single crystals on Au.

(J) DFT calculated the minimum energy path for the dissociation of Se_2 dimers into Se atoms and the Se atom diffusion on Au(111). Reprinted with permission from Gao et al. (2017). Copyright 2017, John Wiley & Sons, Inc.

a minute difference in their measured values (Budininkas et al., 1968a, 1968b, 1968c; Meschi and Searcy, 1969). The density functional theory (DFT) calculations by Gao et al. show that the energy barrier required in the sulfurization of W_3O_9 is ~0.9 eV lower by S atoms on Au than by S_2 dimers without Au (Gao et al.,

2015). Interestingly, as shown in Figure 6H, the S_2 dissociation on Au is a spontaneous exothermic process with only a small energy barrier of 0.22 eV. Moreover, Gao et al. found that the dissociation of Se_2 dimers into Se atoms was a highly exothermic process releasing much more energy than S_2 dissociation and even requires no energy barrier (Figure 6J) (Gao et al., 2017). Chen et al.'s kinetic Monte Carlo (kMC) simulations revealed that the fast kink nucleation and ultrafast kink propagation along the edge were the direct origins of the ultrafast growth of triangular WSe_2 domains (Chen et al., 2019). Notably, Gao et al. (Gao et al., 2015, 2017) and Chen et al. (Chen et al., 2019) confirmed that the energy barriers for the surface diffusion of a W_2 dimer, S adatom, and Se adatom on Au(111) surface were all very low. Therefore, the nucleation and expansion of monolayer WS_2 or WSe_2 domains prefer to occur on the catalytic Au surface. Furthermore, abundant S or Se adatoms on the Au surface allow complete sulfurization or selenization, reducing the number of S or Se vacancies in the lattice of WS_2 or WSe_2, respectively.

Similarly, the catalytic Au surface can also be used to grow other sulfides and selenides of transition metals and exhibits good controllability of both layer thickness and quality. To date, the growth methods of several 2D TMDCs on Au, such as TaS_2, $TaSe_2$, $ReSe_2$, $PtSe_2$,et al., have been developed (Jiang et al., 2018, 2019, 2019; Shi et al., 2017, 2018, 2019). The vertical heterostructures of 2D materials, such as MoS_2/*h*-BN (Zhang et al., 2017) and graphene/$ReSe_2$ (Xie et al., 2019), can also be successfully synthesized on Au substrates by two-step growth.

HETEROGENEOUS CATALYST-/SOURCE- METAL SUBSTRATE

Only a limited number of 2D species have been prepared by directly using noble metals as homogeneous substrates. Here, we would like to introduce a universal approach for 2D material growth by using heterogeneous substrates. A typical heterogeneous substrate contains a layer of a noble metal or its intermetallic compound serving as the catalyst and the diffusion channel of source atoms, and the other layer of source metal supplying source elements during the growth (Shivayogimath et al., 2019; Ma et al., 2019). By this unique strategy, we can extend the uses of Au substrates for growing a wide range of 2D materials (Shivayogimath et al., 2019) and those of Pt substrates for growing uniform AB- (Bernal-) stacked bilayer graphene (AB-BLG) (Ma et al., 2019).

Au/source-metal substrate

As reviewed above, the controllable growth of several 2D materials on noble metals is based on two notably different growth modes, i.e., surface-mediated mode and segregation-precipitation (graphene growth) or segregation-conversion mode (the growth of 2D binary compound, such as 2D *h*-BN or TMDCs). The former mode is essential for the growth of large-area single-crystalline domains or continuous uniform films comprised of these domains. However, this mechanism is infeasible once the concentration of dissolved source elements is too high in a noble metal substrate or the catalytic activity of the substrate is too low. Thus, the excess source elements tend to be precipitated or converted (such as sulfurized, selenized, or tellurized by chalcogens) into thick layers on the top surface of the noble metal substrate; or, a substrate surface with insufficient catalytic activity can only weakly attract sources to produce islands instead of uniform layers by the Frank-van der Merwe model (Venables, 2000). The latter mode requires an appreciable concentration of source atoms dissolving in noble metals, followed by the segregation and precipitation/conversion of source atoms. However, the segregation-precipitation/-conversion mode typically leads to the growth of 2D films with poor thickness controllability due to the difficulty in precisely controlling diffusion and precipitation/conversion of dissolved source elements.

The above two growth modes have a crucial step in common, i.e., the diffusion of source atoms. All growth steps of surface-mediated growth, including the surface diffusion of adatoms, occur on the substrate surface. In contrast, segregation-precipitation/-conversion growth involves the inner diffusion of source atoms underneath the top surface of the substrate. Even with the high solubility of source atoms in substrates, surface-mediated growth can still be achieved if the diffusion step is deliberately controlled. For instance, the solubility of Mo atoms in Au (~1 atomic% at 800°C) (Massalski et al., 1986) is much higher than W solubility (below 0.1 atomic% at 800°C) (Okamoto and Massalski, 1985), but strictly monolayer MoS_2 can still grow on Au foils over a wide range of temperatures under low pressure (Shi et al., 2014, 2015a, 2015b). This result is understandable because dissolving is a kinetic rather than a thermodynamic process. Low pressure enables only a negligible amount of Mo atoms to dissolve into Au foil within a limited growth time, restricting the diffusion of Mo atoms to the top surface rather than the inside of the Au substrate.

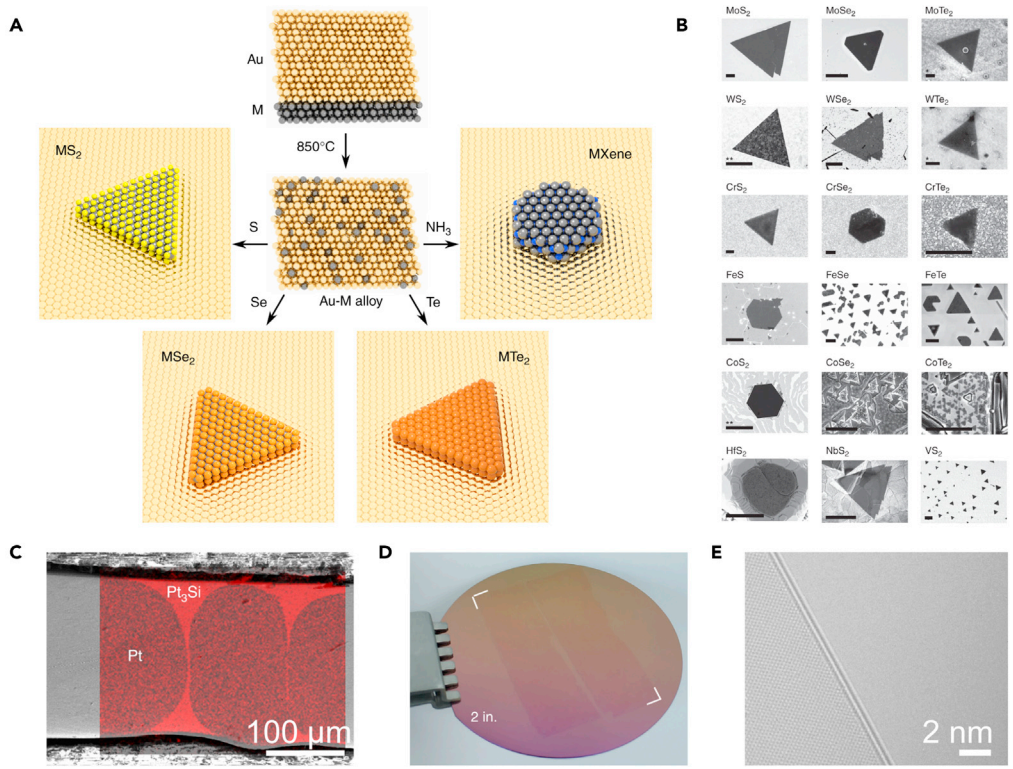

Figure 7. 2D binary compound growth on Au/*M* heterogeneous substrates

(A) Schematic of the synthesis process of 2D binary compounds and (B) SEM images of overall layered transition metal chalcogenides using the Au/*M* heterogeneous substrates (scale bar, 1 μm except where marked: *: 100 nm, **: 10 μm). Reprinted with permission from Shivayogimath et al. (2019). Copyright 2019, Springer Nature.

(C–E) Wafer-scale AB-BLG growth on Pt_3Si/Pt heterogeneous substrate. (C) Overlapping image of an SEM image and an EDS map of the cross-section of the substrate showing a shell-core structure. (D) Photography of two AB-BLG films transferred on a 2-inch SiO_2/Si wafer. (E) High-resolution transmission electron microscopy (HRTEM) showing the graphene film is bilayer. Reprinted with permission from Ma et al. (2019). Copyright 2019, Springer Nature.

It is needed to point out that the two steps, i.e., source diffusion and surface formation of a 2D material, occur in the same or nearly the same sites when using a homogeneous noble metal substrate. Hence, a practical and universal strategy for controlling the diffusion step is to separate its sites from where the surface formation occurs by using a heterogeneous substrate instead. Here we still consider the example of MoS_2 growth to achieve a good thickness control. In the two-step growth of few-layer MoS_2 films, the direct exposure of Au in $Mo(CO)_6$ vapor causes the formation of the Mo-Au surface alloy (Song et al., 2014). As a result, the highest Mo concentration exits in the topmost Au layer (Song and Choi, 2019). However, if the location of Mo supply is shifted away from the top surface of the Au layer (Song et al., 2014) to its bottom surface (Shivayogimath et al., 2019), the Mo concentration in the topmost Au layer still keeps very low due to the presence of a concentration gradient. By such a small but essential change, the saturation or oversaturation of Mo content in the topmost Au layer can be avoided despite the high solubility of Mo in Au, allowing surface-mediated growth or even self-limited growth (Shivayogimath et al., 2019).

Shivayogimath et al. developed a universal approach for the synthesis of 20 binary MX_n (*M* represents metal and *X* represents nonmetal) compounds using Au/source-metal substrates (Figures 7A and 7B) (Shivayogimath et al., 2019). These grown materials cover a wide range of 2D materials, including sulfides (MoS_2, WS_2, CrS_2, HfS_2, et al.), selenides ($MoSe_2$, WSe_2, $CrSe_2$, $CoSe_2$, et al.), tellurides ($MoTe_2$, WTe_2, $CrTe_2$, FeTe, et al.), and even nitride *MX*enes (VN and TaN). The substrates were typically prepared by sputtering a ~20-nm layer of metal *M* on sapphire and a ~500-nm layer of Au on top. Similar to the MoS_2 growth on Au mentioned above (Song et al., 2014; Shivayogimath et al., 2019), the diffusion route of *M* atoms changes due to the shifted *M* supply when using a heterogeneous substrate. Specifically speaking, the surface

diffusion of source-metal atoms on a homogeneous substrate in conventional surface-mediated growth can be changed to the inner diffusion through the Au layer by using a heterogeneous substrate, similar to but not the same as that in segregation-precipitation/-conversion growth where the diffusion route is much shorter and very close to the surface formation sites of the 2D material. The Au diffusion channel of the heterogeneous substrate limits the amount of metal *M* available to a low level in the topmost Au layer, and thus the available growth of 2D MX_n on Au requires no insolubility of metal *M* in Au (Shivayogimath et al., 2019).

Importantly, this approach also shows potential for growing large-area uniform films of 2D non-layered materials such as VN and TaN besides 2D layered materials (Shivayogimath et al., 2019). In the conventional surface-mediated growth of a 2D non-layered binary material, the top surface of the pre-formed 2D material strongly attracts both metal and nonmetal sources from the growth atmosphere due to the presence of surface dangling bonds. As a result, their thickness continuously increases with prolonging the growth time, and thus thickness control becomes difficult. By using a heterogeneous substrate, in contrast, the two different sources, i.e., metal and nonmetal, keep separated until they meet on the Au top surface. The final formation of the 2D material is confined only at the solid-gas interface, and thus excellent thickness control of a wide range of 2D binary materials can be achieved.

Similarly, Sun et al. synthesized high-quality 2D Mo_2C and graphene/Mo_2C on Au/Mo substrates and investigated their HER performance (Sun et al., 2019). The overpotential of the graphene/Mo_2C vertical heterostructure is 249 mV, lower than that of pure Mo_2C crystals. Zhang et al. successfully demonstrated the twinned growth of ReS_2/WS_2 hetero-bilayers on a re-solidified Au substrate supported with a W-Re alloy foil (Zhang et al., 2016). The W-Re alloy foil serves as both the metal sources of ReS_2 and WS_2 monolayers. These works greatly extend the uses of Au substrates for 2D material growth.

Pt_3Si/Pt substrate

We have discussed the uses of pure Pt substrates for graphene growth in the last section and pointed out that the outstanding catalytic activity of Pt can only be fully realized for the thickness control in monolayer graphene growth under matching growth conditions and with rational strategies (Gao et al., 2012; Ma et al., 2014b). The crucial step is to prevent excess carbon atoms from segregation and precipitation on the Pt surface. Such quasi-equilibrium growth allows the growth of large-area uniform monolayer graphene but also prevents the formation of the second- and third-layer graphene (Wang et al., 2018). Thus, a more sophisticated control is highly desired for growing large-area bilayer graphene.

Based on the similar principles of designing Au/source-metal substrates, the concept of the heterogeneous substrates can be extended to a design of shell-core structural Pt_3Si/Pt substrates (Figure 7C) for the CVD growth of uniform AB-BLG (Ma et al., 2019). The liquid Pt_3Si shell has high catalytic activity and relatively low carbon solubility and therefore is used as "the catalyst-metal layer" through where carbon atoms diffuse, followed by the surface growth of graphene layers on its top surface. On the other hand, the solid Pt core is used as "the source-metal layer" to continuously supply carbon atoms due to its relatively high carbon solubility. Here we only concentrate on the thickness control of in bilayer graphene growth in this section and discuss the causes for the large coverage ratio of AB-stacked area, which is strongly dependent on the unique properties of the liquid Pt_3Si surface in the next section.

Babenko et al. first found that the growth rates of graphene domains on silicidated Pt foils were notably higher than those on pristine polycrystalline Pt foils (Babenko et al., 2015). Besides, the sizes of graphene domains on these silicidated substrates were increased, and their hexagonality and uniformity were also improved, compared with those on pristine Pt. These findings indicate that silicidated Pt is a suitable surface catalyst to grow monolayer graphene. Next, Ma et al. successfully achieved the growth of wafer-scale continuous AB-BLG films on similar Pt_3Si/Pt substrates but with a significantly different strategy combining both roles of Pt_3Si and Pt layers (Ma et al., 2019). The unique Pt_3Si/Pt substrates show the outstanding controllability of both the layer number and the stacking order of graphene bilayers. Both coverage ratios of bilayer regions in the grown graphene films and AB-stacked regions in the bilayer graphene films achieved perfection, up to 100%. Under rationally designed growth conditions, wafer-scale AB-BLG films with milliliter-sized graphene grains finally covered the entire substrate surface (Figures 7D and 7E). Both mechanical and electrical properties of these AB-BLG films were comparable to those of mechanically exfoliated AB-BLG samples, indicated by a high 2D Young's modulus up to 684 N m^{-1}, 2D strength of 82 N

m^{-1}, and high carrier mobility up to ~2,100 $cm^2 V^{-1} s^{-1}$. It is worth noting that a widely tunable bandgap exists in mechanically exfoliated bilayer graphene but only in AB-stacked form (Zhang et al., 2009). Notably, a bandgap >26 meV was also observed in the large-sized dual-gate FET devices based on the grown AB-BLG when the displacement field *D* increased to 1.0 V nm^{-1}, strongly confirming their excellent crystallinity in terms of stacking order.

The detailed growth process of graphene bilayers was systematically studied by Ma et al. using carbon isotope labeling technology and DFT calculations (Ma et al., 2019). The whole growth process includes two different stages to grow the first- and second-layer graphene, respectively. During the first 10 min of the growth, the first graphene layer was formed on the Pt_3Si surface at 1100°C, showing a typical self-limited growth behavior similar to monolayer graphene growth on pure Pt substrates (Gao et al., 2012). As the first-layer domains expanded and finally screened the entire Pt_3Si surface, carbon atoms were dissolved and reserved in the Pt core for the next-stage growth, i.e., the epitaxial growth of the second-layer graphene. Then, the carbon supply from the growth atmosphere was ceased due to the presence of the continuous first-layer graphene film with very few defects through which the gaseous carbon source could easily permeate. Then, under a rational cooling rate, the dissolved carbon atoms were continuously released from the Pt core back into the Pt_3Si shell, diffused through the Pt_3Si channel to reach the Pt_3Si top surface, and were then used to grow the second layer. Next, these domains were stitched together into a continuous graphene film underneath the first-layer graphene film. Finally, a bilayer film entirely covered the entire Pt_3Si surface.

It is essential to point out that, during the growth of the first- and the second-layer graphene, the carbon supply and the diffusion modes of carbon atoms are shifted from the gaseous carbon source in the growth atmosphere and the surface diffusion on Pt_3Si for the first-layer growth to the dissolved carbon in carbon-rich Pt core and inner diffusion inside the carbon-poor Pt_3Si shell for the second-layer growth, respectively. The resulting unique growth mode of the second layer leads to the precise control of layer numbers in the bilayer graphene growth on Pt_3Si/Pt. By comparison, it can be seen that the roles of the Pt_3Si shell and the Pt core in the second-layer growth of AB-BLG (Ma et al., 2019) are similar to those of the Au layer and source-metal layer in the TMDC monolayer growth, respectively, when using Au/source-metal substrates (Shivayogimath et al., 2019). Similar heterogeneous substrates were also proposed by Ma et al. to grow uniform graphene multilayers with precise thickness control, using other stoichiometric intermetallic compounds as the diffusion channels (Ma et al., 2019). The graphene growth on Pd_5Si/Pd was also experimentally demonstrated, showing similar AB-BLG results to those using Pt_3Si/Pt.

SURFACE-ENGINEERED SUBSTRATE

Both noble and non-noble metal substrates are metallic. Therefore, all surface engineering strategies, which have ever been used in non-noble metals for 2D material growth, can also be applied to noble metals in principles. Surface engineering is to change the surface morphology of noble metal surfaces for improving the structural uniformity of the grown 2D materials.

Surface roughness

A surface with significantly low roughness is usually smooth with very few surface defects. According to the crystallography fundamentals and many experimental results (Venables, 2000), surface defects can act as preferred nucleation sites for the surface growth of crystals. For instance, random point defects can trap adatoms and thus increase nucleation rate. Therefore, lowering surface roughness to a significant level can reduce nucleation density and increase domain sizes for 2D material growth. Mechanical polishing and electrochemical polishing are two main polishing methods and directly lead to a decrease in macroscopic surface roughness by removing macroscopic surface imperfections such as scratches. In contrast, thermal annealing causes surface reorganization and improves the crystallinity of metal surfaces by removing microscopic surface irregularities such as grain boundaries and dislocations, thus decreasing the microscopic surface roughness.

Polishing (Gao et al., 2013; Kim et al., 2012) and annealing (Li et al., 2009; Song et al., 2010) processes have been widely used to improve 2D material growth since the earliest studies on the CVD growth of graphene (Li et al., 2009; Yu et al., 2008) and 2D *h*-BN (Song et al., 2010). In the first report of graphene growth by CVD in 2008, Yu et al. pointed out that smoother Ni surfaces after the annealing process led to the fabrication of thinner and more uniform graphene (Yu et al., 2008). Furthermore, systematic studies

revealed that a reduction in Cu substrate surface roughness caused a dramatic decrease in the nucleation density (Hedayat et al., 2017) and increased domain sizes of graphene (Braeuninger-Weimer et al., 2016) and *h*-BN (Tay et al., 2014) by comparing their CVD growth using Cu substrates with different roughness. Moreover, these changes in substrates also notably improved the crystalline quality of graphene, indicated by an enhancement of electrical (Griep et al., 2016; Luo et al., 2011) and mechanical (Griep et al., 2016) properties.

Like non-noble metal substrates, polishing and pre-annealing processes can move surface imperfections of noble metals and have become indispensable steps before the CVD growth of large-size 2D crystals using noble metal substrates, such as monolayer *h*-BN or graphene on Pt (Park et al., 2014; Wang et al., 2018) and monolayer WS_2 or WSe_2 on Au (Gao et al., 2015, 2017). In addition, the pre-annealing process is particularly essential in the repeated growth of 2D materials on reusable soft noble metals such as Au. Because the soft surface usually becomes rough after growth and transfer and can be recovered back to its flat state again by a post-annealing process (Gao et al., 2015).

Single-crystalline surface

As noted above, the noble metal substrates used for CVD growth of 2D materials in pioneer reports were the most readily accessible polycrystalline noble metal foils (Gao et al., 2011, 2012, 2013, 2015; Kim et al., 2013; Shi et al., 2014) or films (Kang et al., 2009) rather than single-crystalline noble metals. Also, these substrates were usually polished and annealed before further use for 2D material growth. During long-time annealing, grains of noble metal substrates can grow to a millimeter or even larger scale, and substrate surfaces recrystallize, providing a possibility to investigate the crystallography effect of different facet orientations on 2D material growth using polycrystalline noble metal substrates with large-sized grains. For instance, continuous graphene preferred to grow on Pt(100) and Pt(111) facets, and graphene was rarely found on Pt(311) due to the large lattice mismatch effect (Gao et al., 2011). Thick and thin *h*-BN films were grown on Pt(111) and Pt(001), respectively, under moderate pressure by LPCVD (Park et al., 2014). The domains of monolayer MoS_2 were larger on Au(100) and Au(110) facets than on Au(111) (Shi et al., 2015b). These findings indicate that the crystalline orientation of facets on noble metal surfaces is crucial for the precise control of the thickness, continuity, and uniformity of 2D materials.

Unlike various oriented facets forming the surface of a polycrystalline substrate, a large-area continuous facet with only a single crystallographic orientation becomes the entire surface of the single-crystalline noble metal. This factor may lead to the aligned growth of 2D single-crystalline domains or even highly oriented 2D films. Yang et al. reported the growth of wafer-scale MoS_2 monolayer films stitched from highly oriented MoS_2 domains using single-crystalline Au(111) films as growth substrates (Figure 8A) (Yang et al., 2020). They found a crystal symmetry match between MoS_2 and Au(111) with large-area uniform moiré patterns and a step-guided growth mode from Au<110> steps. Therefore, the structural continuity and orientation uniformity of MoS_2 films were attributed to the homogeneous nucleation of MoS_2 domains along step edges and their alignment with the lattice of Au(111), respectively. In contrast, only misaligned $MoSe_2$ domains were synthesized on Au(100) due to the weak coupling between monolayer $MoSe_2$ and Au(100), and thus the grown monolayer $MoSe_2$ films were still polycrystalline (Figure 8C) (Wu et al., 2021). Very recently, single-orientated graphene domains and their stitched films were also demonstrated using twined Pt(111) as the growth substrate (Figure 8B) (Kang et al., 2021).

Liquid surface

A liquid surface has multiple unique characterizations distinct from a solid surface. The two most important are the ultrasmooth and noncrystalline structure and the excellent rheology (Liu and Fu, 2019; Zeng and Fu, 2018), allowing for many advantages in the 2D material growth, which are difficult or even impossible to realize on their solids. Here we discuss how these two unique characterizations of liquid surfaces influence the growth of 2D materials using noble metals.

It is widely known that a liquid at rest keeps an ultra-flat top surface due to the gravity pulling on liquid atoms or molecules and the fluidity recovering its flatness from its deformation rapidly. Polishing and annealing can reduce the roughness of a solid metal substrate to a certain extent, and the mono-crystallization process can eliminate grain boundaries to form a single-crystalline surface. However, many morphology irregularities such as steps and dislocations still exist on single- and polycrystalline substrates, leading to a high nucleation density of 2D materials on these inhomogeneous defect sites. In contrast, the

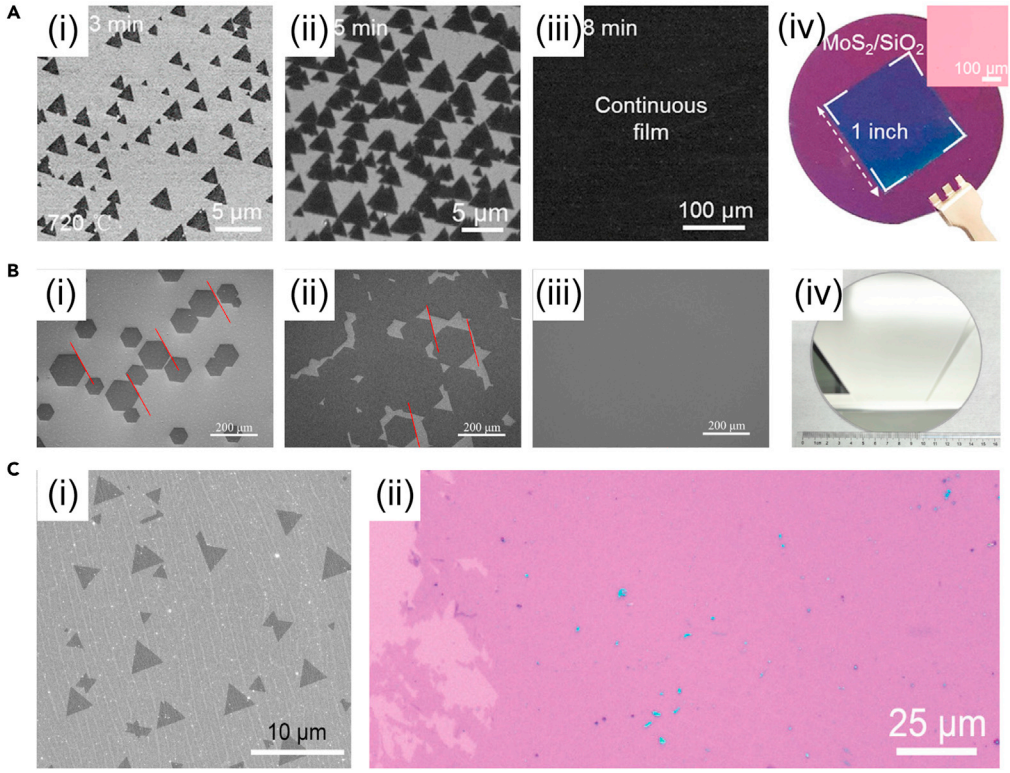

Figure 8. 2D material growth on single-crystalline Au and Pt

(A) Aligned MoS_2 domains (i) expanded, (ii) joined up, and finally (iii) formed a continuous film on Au(111) with prolonging the growth time. (iv) Photography and OM image (inset) of a 1-inch monolayer MoS_2 film transferred on a SiO_2/Si wafer. Reprinted with permission from Yang et al. (2020). Copyright 2020, American Chemical Society.

(B) Aligned graphene domains (i) expanded, (ii) joined up, and finally (iii) formed a continuous film on Pt(111) with prolonging the growth time. (iv) Photography of 6-inch single-crystal graphene on Pt(111). Reprinted with permission from Kang et al., 2021. Copyright 2021, Elsevier.

(C) Monolayer $MoSe_2$ growth on Au(100). (i) SEM image of misaligned $MoSe_2$ domains on a (100)-faceted Au foil. (ii) OM image of monolayer $MoSe_2$ transferred on SiO_2/Si. Reprinted with permission from Wu et al. (2021). Copyright 2021, American Chemical Society.

surface of a liquid metal substrate is ultrasmooth to a quasi-atomic level. Its structure can be described as an assembly of metal atoms with long-range disorder and short-range order based on the random-packing model (Finney and Bernal, 1970). Therefore, almost all crystallographic defects on a solid surface, such as boundaries, are absent on a liquid surface, dramatically reducing the nucleation density of 2D materials in CVD growth.

Nevertheless, vacancies are still randomly distributed on a liquid surface as a structural imperfection in a short-range order (Wagner, 1977). The highly isotropic noncrystalline structure of the liquid surface allows homogeneous nucleation of 2D materials on these defect sites. Therefore, 2D domains with similar sizes are seamlessly stitched into a uniform continuous film (Geng et al., 2012). In addition, adatoms can diffuse very fast on such an ultrasmooth surface. As a result, low nucleation density and high growth rate of 2D materials can be achieved on liquid surfaces at high growth temperatures, especially those of substrates with high catalytic activity, such as liquefied noble metals (Babenko et al., 2015; Lee et al., 2018). For instance, the nucleation density of the graphene domain is only 0.3 mm^{-2} on liquid Pt_3Si, about 1.5 times that on solid pristine Pt (Babenko et al., 2015). Also, the liquid Pt_3Si surface enhanced the growth rate of monolayer graphene domains an order of magnitude higher than the solid Pt surface, up to 120 and 133 μm min^{-1} reported by Babenko et al. (Figure 9C), and Ma et al. (the first-layer graphene) respectively (Babenko et al., 2015; Ma et al., 2019). The similar speeding-up effect of liquefied metals on monolayer *h*-BN growth was also demonstrated by Lee et al. using liquid Au (Lee et al., 2018).

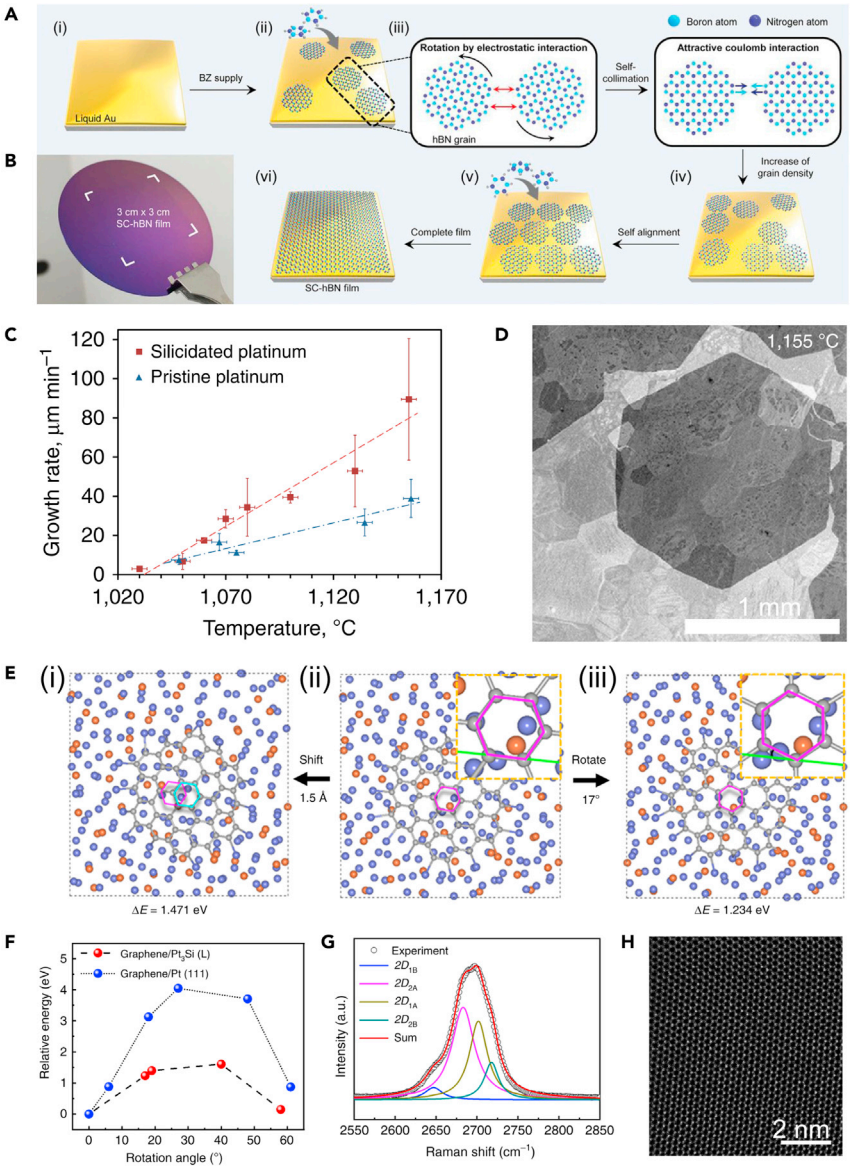

Figure 9. 2D material growth on liquid Au and liquid Pt_3Si/Pt

(A) Schematic of single-crystal *h*-BN film growth on a liquid Au surface through the self-collimation of *h*-BN grains invoked by the attractive Coulomb interaction.

(B) Photography of a wafer-scale single-crystal *h*-BN film transferred on a SiO_2/Si wafer. Reprinted with permission from Lee et al. (2018). Copyright 2018, American Association for the Advancement of Science.

(C) Comparison between the growth rates of graphene domains on a liquid Pt_3Si surface and a pristine solid Pt surface as functions of temperature.

(D) Representative SEM image of a millimeter-sized graphene domain on Pt_3Si/Pt. Reprinted with permission from Babenko et al. (2015). Copyright 2015, Springer Nature.

(E) Diagrams of representative atomic structures of a graphene nucleus on a liquid Pt_3Si surface at 1500K. The graphene nucleus can be (i) shifted by a distance and (iii) rotated by an angle from (ii) its original position.

(F) Comparison between the relative energies of graphene nuclei on liquid Pt_3Si and solid Pt(111) surfaces as a function of rotation angles at 1500K.

(G) 2*D* Raman peak of the AB-BLG film. The fit of four Lorentzian peaks is shown.

(H) Atomic resolution of scanning transmission electron microscopy (STEM) image of the AB-BLG film. Reprinted with permission from Ma et al. (2019). Copyright 2015, Springer Nature.

Besides the better structural controllability of 2D materials on a liquid surface than on a solid surface mentioned above, the self-assembly manner of 2D materials due to the excellent rheological properties of liquid noble metals is more of a concern, which solid substrates are unlikely to achieve. The self-assembly of 2D materials has two different ways. One is the in-plane self-collimation of 2D domains induced by the attractive electrostatic interaction of edges (Lee et al., 2018). The other is the vertical lattice matching of different 2D layers due to their interlayer epitaxy and a week potential field of the underneath liquid surface (Ma et al., 2019).

Lee et al. reported the wafer-scale growth of single-crystal *h*-BN films on liquid Au surface (Figures 9A and 9B) (Lee et al., 2018). With prolonging growth time, the *h*-BN domains were closely packed. The two adjacent randomly oriented *h*-BN domains were attracted by the Coulomb interaction of their B and N edges but would be anchored if using solid substrates. However, as shown in Figure 9A, the rheological Au surface allows the rotation and translation of *h*-BN domains that float above it. Therefore, a self-collimation and a seamless stitch of *h*-BN domains were achieved due to a combined action of the electrostatic attraction of *h*-BN domain edges and the excellent rheological property of liquid Au. It is essential to point out that, besides the formation mechanism, the structure of a single-crystal 2D film via self-collimated grain formation on a liquid surface differs hugely from that of a highly oriented 2D film via the lattice alignment with the underneath single-crystalline surface. The former is a genuine 2D single crystal without grain boundaries by perfectly collimating the lattices of adjacent 2D grains (Lee et al., 2018). However, the latter is an imperfect "single-crystalline" film with a preferred crystallographic orientation (Yang et al., 2020). For instance, a small proportion of misaligned MoS_2 grains still existed on single-crystalline Au(111) (Yang et al., 2020). As well known, a perfect single-crystalline surface is unlikely to be obtained since crystalline defects such as steps and dislocations always exist. Therefore, the epitaxial 2D domains can only be imperfectly stitched. Even coalesced 2D grains with the same in-plane crystalline orientation are still separated by translational grain boundaries as they are anchored on the solid substrates with poor rheology (Chubarov et al., 2021; Hickey et al., 2021).

As noted in the last section, the graphene bilayers obtained on Pt_3Si/Pt are perfectly AB stacked (Ma et al., 2019). The lattice of pre-formed first-layer graphene rather than the underneath substrate determines the lattice orientation of the post-formed second-layer graphene. The DFT calculations by Ma et al. revealed that the energy changes caused by the rotation and translation of a graphene nucleus on liquid Pt_3Si were both much lower than those on solid Pt(111), as shown in Figures 9E and 9F, but the binding strength of graphene nuclei with these two different substrates was very close (Ma et al., 2019). Moreover, after geometry relaxation, the liquid Pt_3Si lattice showed a self-adjusting manner when the graphene nucleus was shifted by a small distance or rotated by an angle (Figure 9E), revealing the typical rheological characteristic of liquid Pt_3Si influenced by the graphene nucleus movements. These results strongly confirm the significant effects of rheological liquid substrates on the interlayer epitaxy of bilayers, enabling the weak van der Waals potential to dominate the self-adjusting rotation and translation processes of the 2D nuclei of the post-formed layers. Thus, a 100% coverage ratio of AB-stacked regions in bilayer graphene was achieved (Figures 9G and 9H), and the area of the second layer was dependent on that of the first layer. In contrast, the AB-stacked regions are usually discontinuous or even absent in bilayer graphene using solid metal substrates (Hao et al., 2016; Liu et al., 2012a; Peng et al., 2011; Zhou et al., 2013).

PROPERTY & APPLICATIONS

Many efforts have been dedicated to the CVD growth methods of diverse 2D materials using noble metals. Considerable numbers of these grown materials are of high crystalline quality and structural uniformity and show excellent properties in electronics, optoelectronics, catalysis, and barrier property (Table 1). This section summarizes these properties and discusses the potential applications of these 2D materials, mainly relying on two classes of properties, i.e., the natural properties of pure 2D products such as transport properties (Gao et al., 2012, 2015, 2017; Ma et al., 2014b), and the combined actions of both the properties of growth substrates and as-grown 2D materials, such as HER properties (Shi et al., 2014, 2017). Then, some possible improvements on synthesis are concluded for large-area applications.

CVD-grown graphene using Pt (Gao et al., 2012; Ma et al., 2014b) and Pt_3Si/Pt (Babenko et al., 2015; Ma et al., 2019) substrates shows outstanding transport properties comparable to those of mechanically exfoliated samples, and therefore have great potential to be scaled up for the applications which have ever

Table 1. Summary of the representative CVD-grown 2D materials using noble metal substrates

Noble metal	2D material	Substrate design	Morphology	Performance	Reference
Au	Gr	polycrystalline Au foil	monolayer films with pronounced *D* peaks	FET, mobility ~20 $cm^2 V^{-1} s^{-1}$	Oznuluer et al. (2011)
	h-BN	polycrystalline Au foil	films with tunable thickness from 3.5 to 10.6 nm	DUV photodetector, rejection ratio $R_{220\ nm}/R_{280\ nm} > 10^3$, $R_{200\ nm}/R_{290\ nm} > 10^4$, responsivity 3.4 mA/W at 220 nm	Tan et al. (2020)
		liquid Au/W foil	wafer-scale single-crystal monolayer films	gas-diffusion barrier, WVTR 0.60 g m^{-2} day^{-1}; oxidation-resistant coating for Cu, 300 °C for 1 h	Lee et al. (2018)
	MoS_2	polycrystalline Au foil	strictly monolayer domains with tunable sizes from ~200 nm to 50 μm	HER, Tafel slope 61 mV/dec, exchange current density ~38.1 μA/cm^2, overpotential ~100 mV	Shi et al. (2014)
		50-nm Au film	2–3-layer films or desired pattern	FET, mobility 0.004 $cm^2 V^{-1} s^{-1}$	Song et al. (2014)
		Au(111) film	highly-oriented monolayer domains and films	FET, mobility ~11.2 $cm^2 V^{-1} s^{-1}$, on/off ratio ~7.7×10^5	Yang et al. (2020)
	$MoSe_2$	Au(100) foil	randomly-oriented monolayer domain and films	NM	Wu et al. (2021)
	WS_2	polycrystalline Au foil	mm-sized monolayer single-crystal domains, ~2-inch continuous films	FET, mobility 1-2 $cm^2 V^{-1} s^{-1}$, on/off ratio ~4×10^6 - ~5×10^7	Gao et al. (2015)
			~420 μm monolayer domains	FET, mobility 20 $cm^2 V^{-1} s^{-1}$, on/off ratio ~10^8	Yun et al. (2015)
			monolayer nanosheets with tunable sizes from ~100 to 1,000 nm	HER (~400 nm nanosheet), Tafel slope 100-104 mV/dec, exchange current density ~30.20 μA/cm^2, overpotential 110-120 mV	Zhang et al. (2015)
	WSe_2	polycrystalline Au foil	mm-sized monolayer domains	FET, mobility 143 $cm^2 V^{-1} s^{-1}$, on/off ratio 9×10^6	Gao et al. (2017)
	TaS_2	polycrystalline Au foil	μm-sized domains and 5-cm films with tunable thickness from ~3 to ~350 nm	HER, Tafel slope 33-42 mV/dec, exchange current density 100–179.47 μA/cm^2, overpotential 65-150 mV	Shi et al. (2017)
	$TaSe_2$	polycrystalline Au foil	5-cm monolayer film, flakes with tunable thickness from 0.8 to 150 nm	Charge density wave (CDW), transition temperature ~125 K for monolayer and 90 K for bulk	Shi et al. (2018)
	$PtSe_2$	polycrystalline Au foil	flakes with tunable thickness from 1 to 3 layers	HER (1L flake), Tafel slope 33-38 mV/dec, exchange current density ~215 μA/cm^2, overpotential ~210 mV	Shi et al. (2019)
	$PdSe_2$	polycrystalline Au foil	even-layered ribbons from 2 to 20 layers	FET, hole mobility 0.1 $cm^2 V^{-1} s^{-1}$ (8L ribbon) and 0.9 $cm^2 V^{-1} s^{-1}$ (20L ribbon)	Jiang et al. (2019)
	$ReSe_2$	polycrystalline Au foil	μm-sized monolayer single-crystal domains	NM	Jiang et al. (2018)
	MoS_2/*h*-BN	polycrystalline Au foil	~20 μm single-crystal MoS_2 monolayer domains on a monolayer *h*-BN film	FET, mobility ~11.4 $cm^2 V^{-1} s^{-1}$, on/off ratio 10^7	Zhang et al. (2017)
	Gr/$ReSe_2$	Au foil	μm-sized monolayer ReS_2 domains underneath a graphene film	NM	Xie et al. (2019)
	Mo_2C	Au/Mo heterogeneous foil	~20 μm Mo_2C flakes with 6–14 nm thickness	HER, Tafel slope 75-77 mV/dec, overpotential 340 mV	Sun et al. (2019)
	Gr/Mo_2C	Au/Mo heterogeneous foil	NM	HER, Tafel slope 75-77 mV/dec, overpotential 249 mV	Sun et al. (2019)
	ReS_2/WS_2	Au/W-Re alloy heterogeneous foil	>600 $μm^2$ 100% overlapped ReS_2/WS_2 hetero-bilayer domains	NM	Zhang et al. (2016)
	MX_n	Au/*M* heterogeneous film	20 binary compounds including MoS_2, WS_2, WSe_2, and WTe_2 monolayers	MoS_2-based FET, 4-30 $cm^2 V^{-1} s^{-1}$, on/off ratio 10^3-10^5	Shivayogimath et al. (2019)

(*Continued on next page*)

Table 1. *Continued*

Noble metal	2D material	Substrate design	Morphology	Performance	Reference
Pt	Gr	100-nm Pt film	monolayers with pronounced *D* peaks	NM	Kang et al. (2009)
		polycrystalline Pt foil	1 to 2 layers	NM	Gao et al. (2011)
			1.3 mm single-crystal domains	FET, mobility ~7,100 $cm^2 V^{-1} s^{-1}$	Gao et al. (2012)
			~3 mm single-crystal domains	FET, mobility ~13, 000 $cm^2 V^{-1} s^{-1}$	Ma et al. (2014b)
		liquid Pt_3Si/solid Pt foil	mm-sized single-crystal domains	FET, mobility 5,525 $cm^2 V^{-1} s^{-1}$	Babenko et al. (2015)
			wafer-scale 100% AB-BLG films with 100% coverage and mm-sized grains	dual-gate FET, mobility ~2,100 $cm^2 V^{-1} s^{-1}$, tunable bandgap >26 meV at D = 1.0 V nm^{-1}, on/off ratio ~10; mechanical properties, 2D Young's modulus 684 N m^{-1}, 2D strength N m^{-1}	Ma et al. (2019)
	h-BN	polycrystalline Pt foil	~1 μm monolayer or bilayer domains, 1-inch monolayer or bilayer films	OBG, 6.07, 5.94, 5.84 eV for monolayer, bilayer, and few-layer *h*-BN, respectively	Gao et al. (2013)
			1-inch monolayer films	OBG, 6.06 eV; FET, insulating nature	Kim et al. (2013)
			2-inch monolayer films	NM	Park et al. (2014)
Pd	Gr	polycrystalline Pd foil	monolayer to few-layer flakes	FET, mobility ~3,650 $cm^2 V^{-1} s^{-1}$	Ma et al. (2014a)
Rh	Gr	polycrystalline Rh foil	films with tunable thickness from monolayer to multilayers	NM	Liu et al. (2012b)
Ag	Gr	polycrystalline Ag foil	few-layer films with pronounced *D* peaks	tarnish-resistant coating for Ag against S vapor	Ayhan et al. (2013)

'Gr', graphene; 'NM', not mentioned.

been demonstrated with mechanically exfoliated graphene. For instance, the gapless monolayer graphene or the gapped AB-stacked bilayer graphene with a tunable but still small bandgap may be unsuitable for low-power semiconducting devices. However, the ultrafast carrier dynamics and ultra-broadband light absorption of graphene allow for its attractive applications in high-speed transistors, or photodetectors and bolometers with a broad operation bandwidth (Koppens et al., 2014; Liao et al., 2010; Mittendorff et al., 2013; Nair et al., 2008; Novoselov et al., 2012). It is worth noting that the realizations of these fantastic applications significantly depend on the intrinsic properties of graphene. Therefore, large-area graphene domains or films with ultrahigh crystalline quality and uniform stacking order close to or even the same as those peeled from graphite, such as wafer-scale single-crystal graphene films consisted of monolayers or perfectly AB-, ABA-, ABC-, ABAB-, or ABCA-stacked multilayers, are highly desirable for practical applications.

An essential physical property of CVD-grown 2D *h*-BN using Pt (Gao et al., 2013; Kim et al., 2013; Park et al., 2014) and Au (Tan et al., 2020) is the large optical bandgap (OBG) (Gao et al., 2013; Kim et al., 2013; Tan et al., 2020) consistent with the theoretically calculated value (Blase et al., 1995). Tan et al. demonstrated the high-performance deep-ultraviolet (DUV) photodetectors based on large-area multilayer *h*-BN using Au (Tan et al., 2020). Owing to the high crystalline quality and excellent light absorptions in the DUV range, these devices showed a large detectivity and ultrahigh rejection ratios with a very low dark current. On the other hand, the outstanding thermal and chemical stabilities of bulk *h*-BN (Pierson, 1999) and good flexibility of 2D *h*-BN enables 2D continuous *h*-BN films to be atomically thin corrosion-resistant coatings against high-temperature oxidizing atmospheres or gas barriers against moisture diffusion. These properties have been demonstrated with the wafer-scale single-crystal *h*-BN film grown by CVD using liquid Au and are indeed superior to those of conventional polycrystalline *h*-BN (Lee et al., 2018). The Cu surface coated with such single-crystal *h*-BN film was still smooth and clean after oxidation in air at 300°C, and the water vapor transmission rate (WVTR) of single-crystal *h*-BN film was only 0.60 g m^{-2} day^{-1}. Based on these results, it is reasonable to infer that the corrosion-resistant and barrier

properties can be further improved once using the large-area uniform single-crystal bilayer or multilayer *h*-BN films.

2D binary metal compounds (chalcogenides, nitride, and carbides) have diverse properties primarily based on their chemical compositions and phases, and the large-scale production of these 2D compounds with uniform structures should open up possibilities for their applications in multiple fields. For example, Gao et al. showed ~2-inch flexible FET arrays based on Au-grown monolayer WS_2 films (Gao et al., 2015). Very recently, Yang et al. demonstrated the FET arrays based on their Au(111)-grown high-oriented MoS_2 monolayers showing narrow distributions in carrier mobility and on/off ratio (Yang et al., 2020). However, the demonstrations of scale-up applications are still rare for most 2D binary metal compounds due to the difficulty in obtaining large-area high-quality samples with continuous and uniform structures. Indeed, seamless wafer-scale single-crystal films are ideal for applications of these 2D compounds. Alternatively, high-oriented grain arrays of 2D compounds are also excellent choices if the fabrication process carefully avoids grain boundaries.

A combination of a 2D material with active sites at the edges and in the basal planes and a chemically stable, conducting, and flat noble metal substrate becomes an ideal HER catalyst system (Huan et al., 2019; Jaramillo et al., 2007; Shi et al., 2017). Unlike those materials transferred on conductive substrates, these grown 2D materials directly contact the growth metal with clean interfaces and very low charge-transfer resistances, allowing enhanced HER activity (Shi et al., 2017). As noted in the Homogeneous Noble Metal Substrate Section, the use of Au for the CVD growth of MoS_2 (Shi et al., 2014) was inspired by a much earlier pioneer HER research based on the UHV epitaxially grown MoS_2 on Au (Jaramillo et al., 2007). Thus, the first application for exploring the CVD-grown MoS_2 using Au substrates was naturally HER. Shi et al. found that the nanosized as-grown MoS_2 grains on Au with the largest edge length per unit area showed the highest HER activity among their MoS_2 samples, with a low Tafel slope of 61 mV/decade and a high exchange current density of 38.1 $\mu A/cm^2$. This Tafel slope value is larger than that of 1–3-layer MoS_2 grown on glassy carbon (140–145 mV/decade) (Yu et al., 2014) and pure Au foil (110 mV/dec) (Shi et al., 2017), but still lower than UHV epitaxially grown MoS_2 on Au (55–60 mV/decade). HER activity also was demonstrated in the other 2D material/Au combined systems. These CVD-grown 2D materials on Au include some TMDCs (e.g., WS_2(Zhang et al., 2015), TaS_2 (Shi et al., 2017), $PtSe_2$ (Shi et al., 2019)), Mo_2C (Sun et al., 2019), and graphene/Mo_2C heterostructures (Sun et al., 2019). By comparing the HER performance of these 2D material/Au systems, it can be found that the HER activity depends on both the species and morphology of 2D materials. The lowest Tafel slope was found in $PtSe_2$/Au (33-38 mV/dec) (Shi et al., 2019) and TaS_2/Au (33–42 mV/dec) (Shi et al., 2017) systems. Also, higher coverage samples with smaller 2D domains can provide longer edges per unit area on Au as more active HER sites usually show lower Tafel slope, lower overpotentials, and higher exchange current density (Shi et al., 2014, 2019; Zhang et al., 2015). In summary, for the high catalytic activity of 2D materials grown on noble metals in HER applications, growth strategy, substrate design, and surface engineering should be combined to increase nucleation density and prevent domains from stitched into continuous films. These are distinct from those for the applications of high-quality, uniform 2D structures requiring intrinsic physical properties, such as electronics and optoelectronics. For instance, an approach using polycrystalline Au foils with defective surfaces at a lower growth temperature is more promising to obtain dispersed 2D nanodomains for HER applications than that using highly annealed single-crystalline Au at a higher growth temperature (Shi et al., 2014).

In addition, more works still need to be done to make the most of new growth methods using noble metal substrates. Besides all of these efforts devoted to the 2D material growth, the transfer process and fabrication technology of the devices based on these 2D materials also significantly impact the properties and performances in a large variety of applications, especially those requiring intrinsic properties ever found in mechanically exfoliated samples (Banszerus et al., 2016).

CHALLENGES & PERSPECTIVES

Noble metals have been deliberately chosen as new substrates for CVD growth of 2D materials because of their high catalytic activity, which is indispensable for controllable growth, and high maneuverability in rational design and surface engineering. The excellent catalytic activity of noble metals allows for 2D material growth with both uniform structure and high quality under optimized growth conditions. The design of heterogeneous substrates introduces new variables in the catalytic growth, such as source supply and

diffusion route, providing many opportunities for growing a wide range of 2D materials and further improving the structural controllability of the grown materials with less dependence on experimental conditions. Surface engineering changes the pristine surface morphology of noble metals, dramatically increasing crystalline quality and reducing the nucleation density and disorientation of 2D materials.

However, compared with the most readily accessible Cu, Ni, and SiO_2/Si substrates, the technology for 2D material growth using noble metal has been far from fully understood. To date, the most frequently used forms of noble metal substrates are still polycrystalline foils or films, with only simple treatments such as polishing (Gao et al., 2013, 2015, 2017) and annealing (Gao et al., 2011; Kang et al., 2009; Kim et al., 2013; Park et al., 2014; Shi et al., 2015b) before growth. New types of noble metal substrates based on rational substrate design or surface engineering for 2D material growth have been reported more rarely than those of non-noble metals, especially Cu, Ni, and their alloys. A few key challenges remaining in this technology are listed as follows, together with the perspectives of their solutions.

First, the effective reducing resurface roughness for noble metals is relatively tricky. Conventional electrochemical polishing (Braeuninger-Weimer et al., 2016; Chae et al., 2009; Griep et al., 2016; Hedayat et al., 2017; Luo et al., 2011; Tay et al., 2014; Yan et al., 2012) used for non-noble metals such as Cu and Ni is inapplicable to chemically stable noble metals, leaving mechanical polishing as the only choice as a polishing process. Mechanical polishing, by contrast, is a metallography technology with higher skill requirements and was less commonly used for smoothing metal substrate surfaces (Han et al., 2011; Luo et al., 2011; Yu et al., 2008). Therefore, the pre-annealing treatment was used as the only process for reducing the surface roughness in most of the reports using noble metals (Gao et al., 2011; Kang et al., 2009; Kim et al., 2013; Park et al., 2014; Shi et al., 2015b). Similar to Cu/sapphire for graphene growth (Deng et al., 2017), uniform deposition or epitaxy rather than sputtering (Kang et al., 2009) of noble metals on an ultrasmooth surface like sapphire or SiO_2/Si wafers is a promising way to achieve wafer-scale uniform noble metal films with low roughness. However, available deposition or epitaxy technology still has limitations for noble metals with high melting points such as Pt.

Second, the preparation of large-area single-crystal noble metal films or foils is almost absent compared with that of Cu and Cu/Ni single crystals (Li et al., 2021). Typically, Wu et al. developed a seeded growth technique to prepare over 30 kinds of 30 × 20 cm^2 single-crystal Cu foils with various facets (Wu et al., 2020). Cu(111)/sapphire (Chen et al., 2020; Deng et al., 2017) and Cu-Ni (111)/sapphire (Zhang et al., 2019) wafers, and Cu foils with (100) (Wang et al., 2016), (111) (Nguyen et al., 2015) or (110) (Wang et al., 2019) facet have been used for the macro-sized growth of single-crystal (or to be more precise, single-oriented) graphene (Deng et al., 2017; Nguyen et al., 2015; Wang et al., 2016; Zhang et al., 2019) and *h*-BN (Chen et al., 2020; Wang et al., 2019) monolayers. In contrast, until very recently, a few reports demonstrated the epitaxial growth of wafer-scale single-oriented 2D materials using single-crystal noble metal substrates, such as monolayer graphene on Pt(111) (Kang et al., 2021) and monolayer MoS_2 on Au(111) (Yang et al., 2020), which may be attributed to the difficulty in mono-crystallization of noble metal films and foils but also inadequate study. Nevertheless, Jin et al. developed a mono-crystallizing method to prepare diverse single-crystal metal foils, including noble metals, by the contact-free annealing of commercial polycrystalline foils (Jin et al., 2018). As a result, large grains up to centimeter size with orientations close to (111) were formed on Pt or Pd foils, opening up the possibility of the CVD growth of single-oriented 2D materials using relatively inexpensive single-crystalline noble metal foils.

Finally, besides graphene, *h*-BN, and TMDCs, there is considerable scope for the CVD growth of large-area 2D materials beyond them. The design of Au/source-metal heterogeneous substrates has shown its great potential for the CVD growth of thin layers of various 2D materials, especially non-layered 2D nitrides and carbide *MX*enes (Shivayogimath et al., 2019; Sun et al., 2019), but their large-area uniform films or single-crystal domains have not been achieved. The excellent structural controllability of monolayer *h*-BN (Lee et al., 2018) using liquid Au suggests a careful design of substrates with liquid surfaces may help for the seamless stitching of a large-area continuous film by the domain self-assembly. Besides, more attention should be paid to understanding the opposite process of growth, i.e., the etching process of 2D materials. Alternative to the homogeneous nucleation on the liquid noble metals, a G-rE-RG process may remove small randomly nucleated domains and leave only a few domains with fewer defects expanded to their largest sizes before stitching together (Ma et al., 2014b).

In summary, the explorations of noble metals as the growth substrates are still in their primary stage for the CVD growth of 2D materials. More detailed considerations should be dedicated to integrating the overall advantages of the intrinsic catalytic activity of noble metals, surface structure and morphology, rational growth conditions, and new growth strategies.

ACKNOWLEDGMENTS

This work was supported by National Research Foundation–Competitive Research Program NRF-CRP22-2019-0007 and NRF-CRP21-2018-0007.

AUTHOR CONTRIBUTIONS

Writing – Original Draft, Y.G.; Writing – Review & Editing, Y.G. and Z.L. Funding Acquisition – Y.L. and Z.L.; Supervision – Y.L. and Z.L.

DECLARATION OF INTERESTS

The authors declare no conflict of interest.

REFERENCES

Au, C.-T., Ng, C.-F., and Liao, M.-S. (1999). Methane dissociation and syngas formation on Ru, Os, Rh, Ir, Pd, Pt, Cu, Ag, and Au: a theoretical study. J. Catal. *185*, 12–22.

Ayhan, M.E., Kalita, G., Sharma, S., and Tanemura, M. (2013). Chemical vapor deposition of graphene on silver foil as a tarnish-resistant coating. Phys. Status Solidi.RRL *7*, 1076–1079.

Babenko, V., Murdock, A.T., Koós, A.A., Britton, J., Crossley, A., Holdway, P., Moffat, J., Huang, J., Alexander-Webber, J.A., Nicholas, R.J., et al. (2015). Rapid epitaxy-free graphene synthesis on silicidated polycrystalline platinum. Nat. Commun. *6*, 7536.

Banhart, F., Kotakoski, J., and Krasheninnikov, A.V. (2011). Structural defects in graphene. ACS Nano *5*, 26–41.

Banszerus, L., Schmitz, M., Engels, S., Goldsche, M., Watanabe, K., Taniguchi, T., Beschoten, B., and Stampfer, C. (2016). Ballistic transport exceeding 28 μm in CVD grown graphene. Nano Lett. *16*, 1387–1391.

Blase, X., Rubio, A., Louie, S.G., and Cohen, M.L. (1995). Quasiparticle band structure of bulk hexagonal boron nitride and related systems. Phys. Rev. B *51*, 6868–6875.

Braeuninger-Weimer, P., Brennan, B., Pollard, A.J., and Hofmann, S. (2016). Understanding and controlling Cu-catalyzed graphene nucleation: the role of impurities, roughness, and oxygen scavenging. Chem. Mater. *28*, 8905–8915.

Budininkas, P., Edwards, R.K., and Wahlbeck, P.G. (1968a). Dissociation energies of Group VIa gaseous homonuclear diatomic molecules.I. sulfur. J. Chem. Phys. *48*, 2859–2866.

Budininkas, P., Edwards, R.K., and Wahlbeck, P.G. (1968b). Dissociation energies of Group VIa gaseous homonuclear diatomic molecules. II. selenium. J. Chem. Phys. *48*, 2867–2869.

Budininkas, P., Edwards, R.K., and Wahlbeck, P.G. (1968c). Dissociation energies of Group VIa gaseous homonuclear diatomic molecules. III. tellurium. J. Chem. Phys. *48*, 2870–2873.

Chae, S.J., Güneş, F., Kim, K.K., Kim, E.S., Han, G.H., Kim, S.M., Shin, H.-J., Yoon, S.-M., Choi, J.-Y., Park, M.H., et al. (2009). Synthesis of large-area graphene layers on poly-nickel substrate by chemical vapor deposition: wrinkle formation. Adv. Mater. *21*, 2328–2333.

Chatterjee, S., Luo, Z., Acerce, M., Yates, D.M., Johnson, A.T.C., and Sneddon, L.G. (2011). Chemical vapor deposition of boron nitride nanosheets on metallic substrates via decaborane/ammonia reactions. Chem. Mater. *23*, 4414–4416.

Chen, J.-H., Jang, C., Xiao, S., Ishigami, M., and Fuhrer, M.S. (2008). Intrinsic and extrinsic performance limits of graphene devices on SiO_2. Nat. Nanotechnol. *3*, 206–209.

Chen, P., Zhang, Z., Duan, X., and Duan, X. (2018). Chemical synthesis of two-dimensional atomic crystals, heterostructures and superlattices. Chem. Soc. Rev. *47*, 3129–3151.

Chen, S., Gao, J., Srinivasan, B.M., Zhang, G., Sorkin, V., Hariharaputran, R., and Zhang, Y.-W. (2019). Origin of ultrafast growth of monolayer WSe_2 via chemical vapor deposition. Npj Comput. Mater. *5*, 28.

Chen, T.-A., Chuu, C.-P., Tseng, C.-C., Wen, C.-K., Wong, H.-S.P., Pan, S., Li, R., Chao, T.-A., Chueh, W.-C., Zhang, Y., et al. (2020). Wafer-scale single-crystal hexagonal boron nitride monolayers on Cu (111). Nature *579*, 219–223.

Choi, W., Choudhary, N., Han, G.H., Park, J., Akinwande, D., and Lee, Y.H. (2017). Recent development of two-dimensional transition metal dichalcogenides and their applications. Mater. Today *20*, 116–130.

Chubarov, M., Choudhury, T.H., Hickey, D.R., Bachu, S., Zhang, T., Sebastian, A., Bansal, A., Zhu, H., Trainor, N., Das, S., et al. (2021). Wafer-scale epitaxial growth of unidirectional WS_2 Monolayers on Sapphire. ACS Nano *15*, 2532–2541.

Coleman, J.N., Lotya, M., O'Neill, A., Bergin, S.D., King, P.J., Khan, U., Young, K., Gaucher, A., De, S., Smith, R.J., et al. (2011). Two-dimensional nanosheets produced by liquid exfoliation of layered materials. Science *331*, 568.

Corso, M., Auwärter, W., Muntwiler, M., Tamai, A., Greber, T., and Osterwalder, J. (2004). Boron nitride nanomesh. Science *303*, 217.

Demirci, U.B. (2017). Ammonia borane, a material with exceptional properties for chemical hydrogen storage. Int. J. Hydrog. Energy *42*, 9978–10013.

Deng, B., Pang, Z., Chen, S., Li, X., Meng, C., Li, J., Liu, M., Wu, J., Qi, Y., Dang, W., et al. (2017). Wrinkle-free single-crystal graphene wafer grown on strain-engineered substrates. ACS Nano *11*, 12337–12345.

Fazen, P.J., Remsen, E.E., Beck, J.S., Carroll, P.J., McGhie, A.R., and Sneddon, L.G. (1995). Synthesis, properties, and ceramic conversion reactions of polyborazylene.A high-yield polymeric precursor to boron nitride. Chem. Mater. *7*, 1942–1956.

Ferrari, A.C., Meyer, J.C., Scardaci, V., Casiraghi, C., Lazzeri, M., Mauri, F., Piscanec, S., Jiang, D., Novoselov, K.S., Roth, S., et al. (2006). Raman spectrum of graphene and graphene layers. Phys. Rev. Lett. *97*, 187401.

Finney, J.L., and Bernal, J.D. (1970). Random packings and the structure of simple liquids. I. The geometry of random close packing. Proc. R. Soc. Lond. Math. Phys. Sci. *319*, 479–493.

Fiori, G., Bonaccorso, F., Iannaccone, G., Palacios, T., Neumaier, D., Seabaugh, A., Banerjee, S.K., and Colombo, L. (2014). Electronics based on two-dimensional materials. Nat. Nanotechnol. *9*, 768–779.

Gamo, Y., Nagashima, A., Wakabayashi, M., Terai, M., and Oshima, C. (1997). Atomic structure of monolayer graphite formed on Ni(111). Surf. Sci. *374*, 61–64.

Gao, L., Ren, W., Xu, H., Jin, L., Wang, Z., Ma, T., Ma, L.-P., Zhang, Z., Fu, Q., Peng, L.-M., et al. (2012). Repeated growth and bubbling transfer of graphene with millimetre-size single-crystal grains using platinum. Nat. Commun. *3*, 699.

Gao, T., Xie, S., Gao, Y., Liu, M., Chen, Y., Zhang, Y., and Liu, Z. (2011). Growth and Atomic-Scale Characterizations of graphene on multifaceted textured Pt foils prepared by chemical vapor deposition. ACS Nano *5*, 9194–9201.

Gao, Y., Ren, W., Ma, T., Liu, Z., Zhang, Y., Liu, W.-B., Ma, L.-P., Ma, X., and Cheng, H.-M. (2013). Repeated and controlled growth of monolayer, bilayer and few-layer hexagonal boron nitride on Pt foils. ACS Nano *7*, 5199–5206.

Gao, Y., Liu, Z., Sun, D.-M., Huang, L., Ma, L.-P., Yin, L.-C., Ma, T., Zhang, Z., Ma, X.-L., Peng, L.-M., et al. (2015). Large-area synthesis of high-quality and uniform monolayer WS_2 on reusable Au foils. Nat. Commun. *6*, 8569.

Gao, Y., Hong, Y.-L., Yin, L.-C., Wu, Z., Yang, Z., Chen, M.-L., Liu, Z., Ma, T., Sun, D.-M., Ni, Z., et al. (2017). Ultrafast growth of high-quality monolayer WSe_2 on Au. Adv. Mater. *29*, 1700990.

Geng, D., Wu, B., Guo, Y., Huang, L., Xue, Y., Chen, J., Yu, G., Jiang, L., Hu, W., and Liu, Y. (2012). Uniform hexagonal graphene flakes and films grown on liquid copper surface. Proc. Natl. Acad. Sci. U S A *109*, 7992.

German, E.D., and Sheintuch, M. (2013). Predicting CH_4 dissociation kinetics on metals: trends, sticking coefficients, H tunneling, and kinetic isotope effect. J. Phys. Chem. C *117*, 22811–22826.

Gomez, T., Florez, E., Rodriguez, J.A., and Illas, F. (2011). Reactivity of transition metals (Pd, Pt, Cu, Ag, Au) toward molecular hydrogen dissociation: extended surfaces versus particles supported on TiC(001) or small is not always better and large is not always bad. J. Phys. Chem. C *115*, 11666–11672.

Gregoryanz, E., Sanloup, C., Somayazulu, M., Badro, J., Fiquet, G., Mao, H., and Hemley, R.J. (2004). Synthesis and characterization of a binary noble metal nitride. Nat. Mater. *3*, 294–297.

Griep, M.H., Sandoz-Rosado, E., Tumlin, T.M., and Wetzel, E. (2016). Enhanced graphene mechanical properties through ultrasmooth copper Growth substrates. Nano Lett. *16*, 1657–1662.

Guo, N., Wei, J., Fan, L., Jia, Y., Liang, D., Zhu, H., Wang, K., and Wu, D. (2012). Controllable growth of triangular hexagonal boron nitride domains on copper foils by an improved low-pressure chemical vapor deposition method. Nanotechnology *23*, 415605.

Gutiérrez, H.R., Perea-López, N., Elías, A.L., Berkdemir, A., Wang, B., Lv, R., López-Urías, F., Crespi, V.H., Terrones, H., and Terrones, M. (2013). Extraordinary room-temperature photoluminescence in triangular WS_2 monolayers. Nano Lett. *13*, 3447–3454.

Hamilton, J.C., and Blakely, J.M. (1980). Carbon segregation to single crystal surfaces of Pt, Pd and Co. Surf. Sci. *91*, 199–217.

Han, G.H., Güneş, F., Bae, J.J., Kim, E.S., Chae, S.J., Shin, H.-J., Choi, J.-Y., Pribat, D., and Lee, Y.H. (2011). Influence of copper morphology in forming nucleation seeds for graphene growth. Nano Lett. *11*, 4144–4148.

Han, J., Lee, J.-Y., Kwon, H., and Yeo, J.-S. (2014). Synthesis of wafer-scale hexagonal boron nitride monolayers free of aminoborane nanoparticles by chemical vapor deposition. Nanotechnology *25*, 145604.

Hao, Y., Wang, L., Liu, Y., Chen, H., Wang, X., Tan, C., Nie, S., Suk, J.W., Jiang, T., Liang, T., et al. (2016). Oxygen-activated growth and bandgap tunability of large single-crystal bilayer graphene. Nat. Nanotechnol. *11*, 426–431.

Hedayat, S.M., Karimi-Sabet, J., and Shariaty-Niassar, M. (2017). Evolution effects of the copper surface morphology on the nucleation density and growth of graphene domains at different growth pressures. Appl. Surf. Sci. *399*, 542–550.

Helveg, S., Lauritsen, J.V., Lægsgaard, E., Stensgaard, I., Nørskov, J.K., Clausen, B.S., Topsøe, H., and Besenbacher, F. (2000). Atomic-scale structure of single-layer MoS_2 nanoclusters. Phys. Rev. Lett. *84*, 951–954.

Hickey, D.R., Nayir, N., Chubarov, M., Choudhury, T.H., Bachu, S., Miao, L., Wang, Y., Qian, C., Crespi, V.H., Redwing, J.M., et al. (2021). Illuminating invisible grain boundaries in coalesced single-orientation WS_2 monolayer films. Nano Lett. *21*, 6487–6495.

Horvath-Bordon, E., Riedel, R., Zerr, A., McMillan, P.F., Auffermann, G., Prots, Y., Bronger, W., Kniep, R., and Kroll, P. (2006). High-pressure chemistry of nitride-based materials. Chem. Soc. Rev. *35*, 987–1014.

Hu, X., Björkman, T., Lipsanen, H., Sun, L., and Krasheninnikov, A.V. (2015). Solubility of boron, carbon, and nitrogen in transition metals: getting insight into trends from first-principles calculations. J. Phys. Chem. Lett. *6*, 3263–3268.

Huan, Y., Shi, J., Zhao, G., Yan, X., and Zhang, Y. (2019). 2D Metallic transitional Metal dichalcogenides for electrochemical hydrogen evolution. Energy Technol. *7*, 1801025.

Huang, J.-K., Pu, J., Hsu, C.-L., Chiu, M.-H., Juang, Z.-Y., Chang, Y.-H., Chang, W.-H., Iwasa, Y., Takenobu, T., and Li, L.-J. (2014). Large-area synthesis of highly crystalline WSe_2 monolayers and device applications. ACS Nano *8*, 923–930.

Ismach, A., Chou, H., Ferrer, D.A., Wu, Y., McDonnell, S., Floresca, H.C., Covacevich, A., Pope, C., Piner, R., Kim, M.J., et al. (2012). Toward the controlled synthesis of hexagonal boron nitride films. ACS Nano *6*, 6378–6385.

Jaramillo, T.F., Jørgensen, K.P., Bonde, J., Nielsen, J.H., Horch, S., and Chorkendorff, I. (2007). Identification of active edge sites for electrochemical H_2 evolution from MoS_2 nanocatalysts. Science *317*, 100.

Jiang, S., Hong, M., Wei, W., Zhao, L., Zhang, N., Zhang, Z., Yang, P., Gao, N., Zhou, X., Xie, C., et al. (2018). Direct synthesis and in situ characterization of monolayer parallelogrammic rhenium diselenide on gold foil. Commun.Chem. *1*, 17.

Jiang, S., Xie, C., Gu, Y., Zhang, Q., Wu, X., Sun, Y., Li, W., Shi, Y., Zhao, L., Pan, S., et al. (2019). Anisotropic growth and scanning tunneling microscopy identification of ultrathin even-layered $PdSe_2$ ribbons. Small *15*, 1902789.

Jin, S., Huang, M., Kwon, Y., Zhang, L., Li, B.-W., Oh, S., Dong, J., Luo, D., Biswal, M., Cunning, B.V., et al. (2018). Colossal grain growth yields single-crystal metal foils by contact-free annealing. Science *362*, 1021.

Kang, B.J., Mun, J.H., Hwang, C.Y., and Cho, B.J. (2009). Monolayer graphene growth on sputtered thin film platinum. J. Appl. Phys. *106*, 104309.

Kim, G., Jang, A.-R., Jeong, H.Y., Lee, Z., Kang, D.J., and Shin, H.S. (2013). Growth of high-crystalline, single-layer hexagonal boron Nitride on recyclable platinum foil. Nano Lett. *13*, 1834–1839.

Kang, H., Tang, P., Shu, H., Zhang, Y., Liang, Y., Li, J., Chen, Z., Sui, Y., Hu, S., Wang, S., et al. (2021). Epitaxial growth of wafer scale antioxidant single-crystal graphene on twinned Pt(111). Carbon *181*, 225–233.

Kim, K.K., Hsu, A., Jia, X., Kim, S.M., Shi, Y., Hofmann, M., Nezich, D., Rodriguez-Nieva, J.F., Dresselhaus, M., Palacios, T., et al. (2012). Synthesis of monolayer hexagonal boron nitride on Cu foil using chemical vapor deposition. Nano Lett. *12*, 161–166.

Kim, K.S., Zhao, Y., Jang, H., Lee, S.Y., Kim, J.M., Kim, K.S., Ahn, J.-H., Kim, P., Choi, J.-Y., and Hong, B.H. (2009). Large-scale pattern growth of graphene films for stretchable transparent electrodes. Nature *457*, 706–710.

Kong, D., Wang, H., Cha, J.J., Pasta, M., Koski, K.J., Yao, J., and Cui, Y. (2013). Synthesis of MoS_2 and $MoSe_2$ Films with vertically aligned layers. Nano Lett. *13*, 1341–1347.

Koppens, F.H.L., Mueller, T., Avouris, Ph., Ferrari, A.C., Vitiello, M.S., and Polini, M. (2014). Photodetectors based on graphene, other two-dimensional materials and hybrid systems. Nat. Nanotechnol. *9*, 780–793.

Lee, J.S., Choi, S.H., Yun, S.J., Kim, Y.I., Boandoh, S., Park, J.-H., Shin, B.G., Ko, H., Lee, S.H., Kim, Y.-M., et al. (2018). Wafer-scale single-crystal hexagonal boron nitride film via self-collimated grain formation. Science *362*, 817.

Lee, K.H., Shin, H.-J., Lee, J., Lee, I., Kim, G.-H., Choi, J.-Y., and Kim, S.-W. (2012a). Large-scale synthesis of high-quality hexagonal boron nitride nanosheets for large-area graphene electronics. Nano Lett. *12*, 714–718.

Lee, Y.-H., Zhang, X.-Q., Zhang, W., Chang, M.-T., Lin, C.-T., Chang, K.-D., Yu, Y.-C., Wang, J.T.-W., Chang, C.-S., Li, L.-J., et al. (2012b). Synthesis of large-area MoS_2 atomic layers with chemical vapor deposition. Adv. Mater. *24*, 2320–2325.

Lee, Y.-H., Yu, L., Wang, H., Fang, W., Ling, X., Shi, Y., Lin, C.-T., Huang, J.-K., Chang, M.-T., Chang, C.-S., et al. (2013). Synthesis and transfer of single-layer transition metal disulfides on diverse surfaces. Nano Lett. *13*, 1852–1857.

Li, S., Wang, S., Tang, D.-M., Zhao, W., Xu, H., Chu, L., Bando, Y., Golberg, D., and Eda, G. (2015). Halide-assisted atmospheric pressure growth of large WSe_2 and WS_2 monolayer crystals. Appl. Mater. Today *1*, 60–66.

Li, X., Cai, W., An, J., Kim, S., Nah, J., Yang, D., Piner, R., Velamakanni, A., Jung, I., Tutuc, E., et al. (2009). Large-area synthesis of high-quality and

uniform graphene films on copper foils. Science *324*, 1312.

Li, Y., Sun, L., Liu, H., Wang, Y., and Liu, Z. (2021). Preparation of single-crystal metal substrates for the growth of high-quality two-dimensional materials. Inorg. Chem. Front. *8*, 182–200.

Liao, L., Lin, Y.-C., Bao, M., Cheng, R., Bai, J., Liu, Y., Qu, Y., Wang, K.L., Huang, Y., and Duan, X. (2010). High-speed graphene transistors with a self-aligned nanowire gate. Nature *467*, 305–308.

Lin, Y.-C., Zhang, W., Huang, J.-K., Liu, K.-K., Lee, Y.-H., Liang, C.-T., Chu, C.-W., and Li, L.-J. (2012). Wafer-scale MoS_2 thin layers prepared by MoO_3 sulfurization. Nanoscale *4*, 6637–6641.

Liu, J., and Fu, L. (2019). Controllable growth of graphene on liquid surfaces. Adv. Mater. *31*, 1800690.

Liu, L., Zhou, H., Cheng, R., Yu, W.J., Liu, Y., Chen, Y., Shaw, J., Zhong, X., Huang, Y., and Duan, X. (2012a). High-yield chemical vapor deposition growth of high-quality large-area AB-stacked bilayer graphene. ACS Nano *6*, 8241–8249.

Liu, M., Zhang, Y., Chen, Y., Gao, Y., Gao, T., Ma, D., Ji, Q., Zhang, Y., Li, C., and Liu, Z. (2012b). Thinning segregated graphene layers on high carbon solubility substrates of rhodium foils by tuning the quenching process. ACS Nano *6*, 10581–10589.

Liu, N., Fu, L., Dai, B., Yan, K., Liu, X., Zhao, R., Zhang, Y., and Liu, Z. (2011). Universal segregation growth approach to wafer-size graphene from non-noble metals. Nano Lett. *11*, 297–303.

Liu, W., Kang, J., Sarkar, D., Khatami, Y., Jena, D., and Banerjee, K. (2013). Role of metal contacts in designing high-performance monolayer n-type WSe_2 field effect transistors. Nano Lett. *13*, 1983–1990.

Liu, Y., Wu, J., Hackenberg, K.P., Zhang, J., Wang, Y.M., Yang, Y., Keyshar, K., Gu, J., Ogitsu, T., Vajtai, R., et al. (2017). Self-optimizing, highly surface-active layered metal dichalcogenide catalysts for hydrogen evolution. Nat. Energy *2*, 17127.

Luo, Z., Lu, Y., Singer, D.W., Berck, M.E., Somers, L.A., Goldsmith, B.R., and Johnson, A.T.C. (2011). Effect of substrate roughness and feedstock concentration on growth of wafer-scale graphene at atmospheric pressure. Chem. Mater. *23*, 1441–1447.

Ma, D., Liu, M., Gao, T., Li, C., Sun, J., Nie, Y., Ji, Q., Zhang, Y., Song, X., Zhang, Y., et al. (2014a). High-Quality Monolayer graphene synthesis on Pd foils via the suppression of multilayer growth at grain boundaries. Small *10*, 4003–4011.

Ma, T., Ren, W., Liu, Z., Huang, L., Ma, L.-P., Ma, X., Zhang, Z., Peng, L.-M., and Cheng, H.-M. (2014b). Repeated growth–etching–regrowth for large-area defect-free single-crystal graphene by chemical vapor deposition. ACS Nano *8*, 12806–12813.

Ma, W., Chen, M.-L., Yin, L., Liu, Z., Li, H., Xu, C., Xin, X., Sun, D.-M., Cheng, H.-M., and Ren, W. (2019). Interlayer epitaxy of wafer-scale high-quality uniform AB-stacked bilayer graphene films on liquid Pt3Si/solid Pt. Nat. Commun. *10*, 2809.

Manzeli, S., Ovchinnikov, D., Pasquier, D., Yazyev, O.V., and Kis, A. (2017). 2D transition metal dichalcogenides. Nat. Rev. Mater. *2*, 17033.

Massalski, T.B., Okamoto, H., and Brewer, L. (1986). The Au–Mo (gold-molybdenum) system. Bull. Alloy Phase Diagr. *7*, 449–452.

Meschi, D.J., and Searcy, A.W. (1969). Investigation of the magnetic moments of S_2, Se_2, Te_2, Se_6, and Se_5 by the Stern–Gerlach magnetic deflection method. J. Chem. Phys. *51*, 5134–5138.

Mittendorff, M., Winnerl, S., Kamann, J., Eroms, J., Weiss, D., Schneider, H., and Helm, M. (2013). Ultrafast graphene-based broadband THz detector. Appl. Phys. Lett. *103*, 021113.

Morozov, S.V., Novoselov, K.S., Katsnelson, M.I., Schedin, F., Elias, D.C., Jaszczak, J.A., and Geim, A.K. (2008). Giant intrinsic carrier mobilities in graphene and its bilayer. Phys. Rev. Lett. *100*, 016602.

Nagashima, A., Tejima, N., Gamou, Y., Kawai, T., and Oshima, C. (1995). Electronic dispersion relations of monolayer hexagonal boron nitride formed on the Ni(111) surface. Phys. Rev. B *51*, 4606–4613.

Nair, R.R., Blake, P., Grigorenko, A.N., Novoselov, K.S., Booth, T.J., Stauber, T., Peres, N.M.R., and Geim, A.K. (2008). Fine structure constant defines visual transparency of graphene. Science *320*, 1308.

Najmaei, S., Liu, Z., Zhou, W., Zou, X., Shi, G., Lei, S., Yakobson, B.I., Idrobo, J.-C., Ajayan, P.M., and Lou, J. (2013). Vapour phase growth and grain boundary structure of molybdenum disulphide atomic layers. Nat. Mater. *12*, 754–759.

Nave, S., and Jackson, B. (2009). Methane dissociation on Ni(111) and Pt(111): energetic and dynamical studies. J. Chem. Phys. *130*, 054701.

Nguyen, V.L., Shin, B.G., Duong, D.L., Kim, S.T., Perello, D., Lim, Y.J., Yuan, Q.H., Ding, F., Jeong, H.Y., Shin, H.S., et al. (2015). Seamless stitching of graphene domains on polished copper (111) foil. Adv. Mater. *27*, 1376–1382.

Novoselov, K.S., Geim, A.K., Morozov, S.V., Jiang, D., Zhang, Y., Dubonos, S.V., Grigorieva, I.V., and Firsov, A.A. (2004). Electric field effect in atomically thin carbon films. Science *306*, 666.

Novoselov, K.S., Jiang, D., Schedin, F., Booth, T.J., Khotkevich, V.V., Morozov, S.V., and Geim, A.K. (2005). Two-dimensional atomic crystals. Proc. Natl. Acad. Sci. U S A *102*, 10451.

Novoselov, K.S., Fal'ko, V.I., Colombo, L., Gellert, P.R., Schwab, M.G., and Kim, K. (2012). A roadmap for graphene. Nature *490*, 192–200.

Okamoto, H., and Massalski, T.B. (1985). The Au–W (Gold-Tungsten) system. Bull. Alloy Phase Diagr. *6*, 136–137.

Oznuluer, T., Pince, E., Polat, E.O., Balci, O., Salihoglu, O., and Kocabas, C. (2011). Synthesis of graphene on gold. Appl. Phys. Lett. *98*, 183101.

Park, J., Mitchel, W.C., Grazulis, L., Smith, H.E., Eyink, K.G., Boeckl, J.J., Tomich, D.H., Pacley, S.D., and Hoelscher, J.E. (2010). Epitaxial graphene growth by carbon molecular beam epitaxy (CMBE). Adv. Mater. *22*, 4140–4145.

Park, J.-H., Park, J.C., Yun, S.J., Kim, H., Luong, D.H., Kim, S.M., Choi, S.H., Yang, W., Kong, J., Kim, K.K., et al. (2014). Large-area monolayer hexagonal boron nitride on Pt foil. ACS Nano *8*, 8520–8528.

Peng, Z., Yan, Z., Sun, Z., and Tour, J.M. (2011). Direct growth of bilayer graphene on SiO_2 substrates by carbon diffusion through nickel. ACS Nano *5*, 8241–8247.

Pierson, H.O. (1999). Handbook of Chemical Vapor Deposition: Principles, Technology and Applications (William Andrew Inc.).

Qin, B., Ma, H., Hossain, M., Zhong, M., Xia, Q., Li, B., and Duan, X. (2020). Substrates in the synthesis of two-dimensional materials via chemical vapor deposition. Chem. Mater. *32*, 10321–10347.

Raty, J.-Y., Gygi, F., and Galli, G. (2005). Growth of carbon nanotubes on metal nanoparticles: a microscopic mechanism from *ab initio* molecular dynamics simulations. Phys. Rev. Lett. *95*, 096103.

Reina, A., Jia, X., Ho, J., Nezich, D., Son, H., Bulovic, V., Dresselhaus, M.S., and Kong, J. (2009). Large area, few-layer graphene films on arbitrary substrates by chemical vapor deposition. Nano Lett. *9*, 30–35.

Shi, J., Ma, D., Han, G.-F., Zhang, Y., Ji, Q., Gao, T., Sun, J., Song, X., Li, C., Zhang, Y., et al. (2014). Controllable growth and transfer of monolayer MoS_2 on Au foils and its potential application in hydrogen evolution reaction. ACS Nano *8*, 10196–10204.

Shi, J., Yang, Y., Zhang, Y., Ma, D., Wei, W., Ji, Q., Zhang, Y., Song, X., Gao, T., Li, C., et al. (2015a). Monolayer MoS_2 growth on Au foils and on-site domain boundary imaging. Adv. Funct. Mater. *25*, 842–849.

Shi, J., Zhang, X., Ma, D., Zhu, J., Zhang, Y., Guo, Z., Yao, Y., Ji, Q., Song, X., Zhang, Y., et al. (2015b). Substrate facet effect on the growth of monolayer MoS_2 on Au foils. ACS Nano *9*, 4017–4025.

Shi, J., Wang, X., Zhang, S., Xiao, L., Huan, Y., Gong, Y., Zhang, Z., Li, Y., Zhou, X., Hong, M., et al. (2017). Two-dimensional metallic tantalum disulfide as a hydrogen evolution catalyst. Nat. Commun. *8*, 958.

Shi, J., Chen, X., Zhao, L., Gong, Y., Hong, M., Huan, Y., Zhang, Z., Yang, P., Li, Y., Zhang, Q., et al. (2018). Chemical vapor deposition grown wafer-scale 2D tantalum diselenide with robust charge-density-wave order. Adv. Mater. *30*, 1804616.

Shi, J., Huan, Y., Hong, M., Xu, R., Yang, P., Zhang, Z., Zou, X., and Zhang, Y. (2019). Chemical vapor deposition grown large-scale atomically thin platinum diselenide with semimetal–semiconductor transition. ACS Nano *13*, 8442–8451.

Shi, Y., Hamsen, C., Jia, X., Kim, K.K., Reina, A., Hofmann, M., Hsu, A.L., Zhang, K., Li, H., Juang, Z.-Y., et al. (2010). Synthesis of few-layer hexagonal boron nitride thin film by chemical vapor deposition. Nano Lett. *10*, 4134–4139.

Shivayogimath, A., Thomsen, J.D., Mackenzie, D.M.A., Geisler, M., Stan, R.-M., Holt, A.J., Bianchi, M., Crovetto, A., Whelan, P.R., Carvalho, A., et al. (2019). A universal approach for the synthesis of two-dimensional binary compounds. Nat. Commun. *10*, 2957.

Somayajulu, G.R. (1960). Dissociation energies of diatomic molecules. J. Chem. Phys. *33*, 1541–1553.

Song, I., and Choi, H.C. (2019). Revealing the role of gold in the growth of two-dimensional molybdenum disulfide by surface alloy formation. Chem. Eur. J. *25*, 2337–2344.

Song, I., Park, C., Hong, M., Baik, J., Shin, H.-J., and Choi, H.C. (2014). Patternable Large-scale molybdenium disulfide atomic layers grown by gold-assisted chemical vapor deposition. Angew. Chem. Int. Ed. *53*, 1266–1269.

Song, L., Ci, L., Lu, H., Sorokin, P.B., Jin, C., Ni, J., Kvashnin, A.G., Kvashnin, D.G., Lou, J., Yakobson, B.I., et al. (2010). Large scale growth and characterization of atomic hexagonal boron nitride layers. Nano Lett. *10*, 3209–3215.

Sun, J., Nam, Y., Lindvall, N., Cole, M.T., Teo, K.B.K., Woo Park, Y., and Yurgens, A. (2014). Growth mechanism of graphene on platinum: surface catalysis and carbon segregation. Appl. Phys. Lett. *104*, 152107.

Sun, W., Wang, X., Feng, J., Li, T., Huan, Y., Qiao, J., He, L., and Ma, D. (2019). Controlled synthesis of 2D Mo_2C/graphene heterostructure on liquid Au substrates as enhanced electrocatalytic electrodes. Nanotechnology *30*, 385601.

Tan, C., and Zhang, H. (2015). Wet-chemical synthesis and applications of non-layer structured two-dimensional nanomaterials. Nat. Commun. *6*, 7873.

Tan, B., Yang, H., Hu, Y., Gao, F., Wang, L., Dai, M., Zhang, S., Shang, H., Chen, H., and Hu, P. (2020). Synthesis of high-quality multilayer hexagonal boron nitride films on Au foils for ultrahigh rejection ratio solar-blind photodetection. ACS Appl. Mater. Interfaces *12*, 28351–28359.

Tay, R.Y., Griep, M.H., Mallick, G., Tsang, S.H., Singh, R.S., Tumlin, T., Teo, E.H.T., and Karna, S.P. (2014). Growth of large single-crystalline two-dimensional boron nitride hexagons on electropolished copper. Nano Lett. *14*, 839–846.

Venables, J.A. (2000). Introduction to Surface and Thin Film Processes (Cambridge University Press).

Wagner, C. (1977). Point defects and their interaction. Annu. Rev. Mater. Sci. *7*, 1–24.

Wang, H., Xu, X., Li, J., Lin, L., Sun, L., Sun, X., Zhao, S., Tan, C., Chen, C., Dang, W., et al. (2016). Surface monocrystallization of copper foil for fast growth of large single-crystal graphene under free molecular flow. Adv. Mater. *28*, 8968–8974.

Wang, J., Li, T., Wang, Q., Wang, W., Shi, R., Wang, N., Amini, A., and Cheng, C. (2020). Controlled growth of atomically thin transition metal dichalcogenides via chemical vapor deposition method. Mater.Today Adv. *8*, 100098.

Wang, L., Xu, X., Zhang, L., Qiao, R., Wu, M., Wang, Z., Zhang, S., Liang, J., Zhang, Z., Zhang, Z., et al. (2019). Epitaxial growth of a 100-square-centimetre single-crystal hexagonal boron nitride monolayer on copper. Nature *570*, 91–95.

Wang, X., Gong, Y., Shi, G., Chow, W.L., Keyshar, K., Ye, G., Vajtai, R., Lou, J., Liu, Z., Ringe, E., et al. (2014). Chemical vapor deposition growth of crystalline monolayer $MoSe_2$. ACS Nano *8*, 5125–5131.

Wang, Z.-J., Ding, F., Eres, G., Antonietti, M., Schloegl, R., and Willinger, M.G. (2018). Formation mechanism, growth kinetics, and stability limits of graphene adlayers in metal-catalyzed CVD growth. Adv. Mater. Interfaces *5*, 1800255.

Wen, Y., Shang, X., Dong, J., Xu, K., He, J., and Jiang, C. (2015). Ultraclean and large-area monolayer hexagonal boron nitride on Cu foil using chemical vapor deposition. Nanotechnology *26*, 275601.

Wolf, G., Baumann, J., Baitalow, F., and Hoffmann, F.P. (2000). Calorimetric process monitoring of thermal decomposition of B–N–H compounds. Thermochim. Acta *343*, 19–25.

Wu, M., Zhang, Z., Xu, X., Zhang, Z., Duan, Y., Dong, J., Qiao, R., You, S., Wang, L., Qi, J., et al. (2020). Seeded growth of large single-crystal copper foils with high-index facets. Nature *581*, 406–410.

Wu, Q., Fu, X., Yang, K., Wu, H., Liu, L., Zhang, L., Tian, Y., Yin, L.-J., Huang, W.-Q., Zhang, W., et al. (2021). Promoting a weak coupling of monolayer $MoSe_2$ grown on (100)-faceted Au foil. ACS Nano *15*, 4481–4489.

Wu, Z., Luo, Z., Shen, Y., Zhao, W., Wang, W., Nan, H., Guo, X., Sun, L., Wang, X., You, Y., et al. (2016). Defects as a factor limiting carrier mobility in WSe_2: a spectroscopic investigation. Nano Res. *9*, 3622–3631.

Xie, C., Jiang, S., Zou, X., Sun, Y., Zhao, L., Hong, M., Chen, S., Huan, Y., Shi, J., Zhou, X., et al. (2019). Space-confined growth of monolayer $ReSe_2$ under a graphene layer on Au foils. Nano Res. *12*, 149–157.

Yan, Z., Lin, J., Peng, Z., Sun, Z., Zhu, Y., Li, L., Xiang, C., Samuel, E.L., Kittrell, C., and Tour, J.M. (2012). Toward the synthesis of wafer-scale single-crystal graphene on copper foils. ACS Nano *6*, 9110–9117.

Yang, P., Zhang, S., Pan, S., Tang, B., Liang, Y., Zhao, X., Zhang, Z., Shi, J., Huan, Y., Shi, Y., et al. (2020). Epitaxial growth of centimeter-scale single-crystal MoS_2 monolayer on Au(111). ACS Nano *14*, 5036–5045.

Yong, V., and Hahn, H.T. (2011). Graphene growth with giant domains using chemical vapor deposition. Cryst.Eng. Comm. *13*, 6933–6936.

Yu, Q., Lian, J., Siriponglert, S., Li, H., Chen, Y.P., and Pei, S.-S. (2008). Graphene segregated on Ni surfaces and transferred to insulators. Appl. Phys. Lett. *93*, 113103.

Yu, Q., Jauregui, L.A., Wu, W., Colby, R., Tian, J., Su, Z., Cao, H., Liu, Z., Pandey, D., Wei, D., et al. (2011). Control and characterization of individual grains and grain boundaries in graphene grown by chemical vapour deposition. Nat. Mater. *10*, 443–449.

Yu, Y., Huang, S.-Y., Li, Y., Steinmann, S.N., Yang, W., and Cao, L. (2014). Layer-dependent electrocatalysis of MoS_2 for hydrogen evolution. Nano Lett. *14*, 553–558.

Yun, S.J., Chae, S.H., Kim, H., Park, J.C., Park, J.-H., Han, G.H., Lee, J.S., Kim, S.M., Oh, H.M., Seok, J., et al. (2015). Synthesis of centimeter-scale monolayer tungsten disulfide film on gold foils. ACS Nano *9*, 5510–5519.

van der Zande, A.M., Huang, P.Y., Chenet, D.A., Berkelbach, T.C., You, Y., Lee, G.-H., Heinz, T.F., Reichman, D.R., Muller, D.A., and Hone, J.C. (2013). Grains and grain boundaries in highly crystalline monolayer molybdenum disulphide. Nat. Mater. *12*, 554–561.

Zeng, M., and Fu, L. (2018). Controllable fabrication of graphene and related two-dimensional materials on liquid metals via chemical vapor deposition. Acc. Chem. Res. *51*, 2839–2847.

Zhan, Y., Liu, Z., Najmaei, S., Ajayan, P.M., and Lou, J. (2012). Large-area vapor-phase growth and characterization of MoS_2 atomic layers on a SiO_2 substrate. Small *8*, 966–971.

Zhang, T., Jiang, B., Xu, Z., Mendes, R.G., Xiao, Y., Chen, L., Fang, L., Gemming, T., Chen, S., Rümmeli, M.H., et al. (2016). Twinned growth behaviour of two-dimensional materials. Nat. Commun. *7*, 13911.

Zhang, X., Wu, T., Jiang, Q., Wang, H., Zhu, H., Chen, Z., Jiang, R., Niu, T., Li, Z., Zhang, Y., et al. (2019). Epitaxial growth of 6 in.Single-crystalline graphene on a Cu/Ni (111) film at 750 °C via Chemical vapor deposition. Small *15*, 1805395.

Zhang, Y., Tang, T.-T., Girit, C., Hao, Z., Martin, M.C., Zettl, A., Crommie, M.F., Shen, Y.R., and Wang, F. (2009). Direct observation of a widely tunable bandgap in bilayer graphene. Nature *459*, 820–823.

Zhang, Y., Shi, J., Han, G., Li, M., Ji, Q., Ma, D., Zhang, Y., Li, C., Lang, X., Zhang, Y., et al. (2015). Chemical vapor deposition of monolayer WS_2 nanosheets on Au foils toward direct application in hydrogen evolution. Nano Res. *8*, 2881–2890.

Zhang, Z., Ji, X., Shi, J., Zhou, X., Zhang, S., Hou, Y., Qi, Y., Fang, Q., Ji, Q., Zhang, Y., et al. (2017). Direct Chemical Vapor Deposition growth and band-gap characterization of MoS_2/h-BN van der Waals heterostructures on Au foils. ACS Nano *11*, 4328–4336.

Zhao, S., Wang, L., and Fu, L. (2019). Precise vapor-phase synthesis of two-dimensional atomic single crystals. iScience *20*, 527–545.

Zhou, H., Yu, W.J., Liu, L., Cheng, R., Chen, Y., Huang, X., Liu, Y., Wang, Y., Huang, Y., and Duan, X. (2013). Chemical vapour deposition growth of large single crystals of monolayer and bilayer graphene. Nat. Commun. *4*, 2096.